Title

Synthetic, Mechanistic, and Biological Interrogation of Ginkgo biloba Chemical Space En Route to (−)-Bilobalide

Journal

Journal of the American Chemical Society, 142(43)

ISSN

0002-7863

Authors

Demoret, Robert M
Baker, Meghan A
Ohtawa, Masaki
et al.

Publication Date

2020-10-28

DOI

10.1021/jacs.0c08231

Peer reviewed

HHS Public Access

Author manuscript

J Am Chem Soc. Author manuscript; available in PMC 2021 October 28.

Published in final edited form as:

J Am Chem Soc. 2020 October 28; 142(43): 18599–18618. doi:10.1021/jacs.0c08231.

Synthetic, Mechanistic and Biological Interrogation of *Ginkgo biloba* Chemical Space en route to (−)-Bilobalide

Robert M. Demoret[1,‡], **Meghan A. Baker**[1,‡], **Masaki Ohtawa**[1,†], **Shuming Chen**[2], **Ching Ching Lam**[2], **Sophia Khom**[4], **Marisa Roberto**[4], **Stefano Forli**[3], **Kendall N. Houk**[2], **Ryan A. Shenvi**[1,*]

[1]Department of Chemistry, Scripps Research, La Jolla, California 92037, United States

[2]Department of Chemistry and Biochemistry, University of California, Los Angeles, CA, USA

[3]DISCoBio, Scripps Research, La Jolla, California 92037, United States

[4]Departments of Molecular Medicine and Neuroscience, La Jolla, California 92037, United States

Abstract

Here we interrogate the structurally dense (1.63 mcbits/Å^3) $GABA_A$ receptor antagonist bilobalide, intermediates en route to its synthesis and related mechanistic questions. ^{13}C isotope labeling identifies an unexpected bromine migration en route to an α-selective, catalytic asymmetric Reformatsky reaction, ruling out an asymmetric allylation pathway. Experiment and computation converge on the driving forces behind two surprising observations. First, an oxetane acetal persists in concentrated mineral acid (1.5 M DCl in THF-d_8/D_2O); its longevity is correlated to destabilizing steric clash between substituents upon ring-opening. Second, a regioselective oxidation of *des*-hydroxybilobalide is found to rely on lactone acidification through lone-pair delocalization, which leads to extremely rapid intermolecular enolate equilibration. We also establish equivalent effects of (−)-bilobalide and the nonconvulsive sesquiterpene (−)-jiadifenolide on action potential-independent inhibitory currents at GABAergic synapses, using (+)-bilobalide as a negative control. The high information density of bilobalide distinguishes it from other scaffolds, and may characterize natural product (NP) space more generally. Therefore, we also include a Python script to quickly (*ca*. 132,000 molecules/minute) calculate information content (Böttcher scores), which may prove helpful to identify important features of NP space.

Graphical Abstract

*Corresponding Author rshenvi@scripps.edu.

†Present Addresses Graduate School of Pharmaceutical Sciences, Kitasato University, Tokyo, Japan

‡Author Contributions These authors contributed equally.

Supporting Information

The Supporting Information is available free of charge on the ACS Publications website.

Experimental materials and methods; computational methods; X-ray crystallography data; python script for Böttcher analysis.

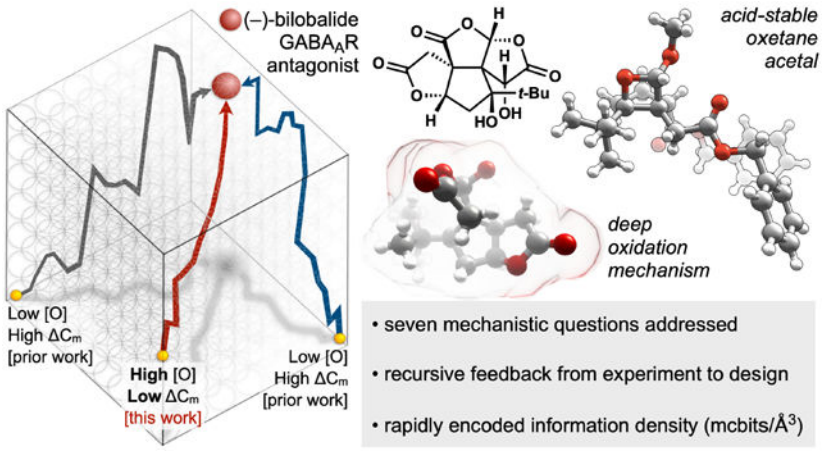

Introduction.

Herbal supplements and remedies constitute a large and controversial market.[1] Not regulated as conventional foods or drugs by the FDA,[2] plant extracts can nevertheless contain orally bioavailable small molecules with profound effects on human biology. Successful sales, however, do not rely on the same demonstrations of efficacy and safety as approved pharmaceuticals. For instance, leaf extracts of *Ginkgo biloba* are widely marketed today as nootropic supplements, but the ability of these extracts to improve cognition is questionable.[3] Despite the ambiguity, approximately 1.6 million adults reported using *G. biloba* extracts in the US in a 2012 survey.[4,5] Even with clear target annotation for several constituents, as well as proven brain penetration,[6] any benefits of *Ginkgo* extracts remain largely unsubstantiated. Additionally, a two-year study by the National Toxicology Program (NTP) concluded that one commercially available *G. Biloba* extract increased rates of liver and thyroid cancers in mice and rats.[7] Adverse events have been long attributed to ingestion of *Gingko* extracts, especially increased bleed time (see below).

Even so, individual components of the crude extract may find useful application if isolated from the off-target activity of congeners. For example, pure bilobalide (−)-**1** exhibited normalization of cognitive impairment in models of Down syndrome, Ts65Dn mice, which exhibit excess inhibitory signaling.[8] Four-week administration of bilobalide led to improved cognitive performance, which correlated to enhanced long-term potentiation (LTP, strengthening of synapses) by a related compound (pentyltetrazole, PTZ) even months after drug regimen had ended. Bilobalide also displayed protection against NMDA-induced excitotoxicity in rat hippocampus.[9]

In addition to human applications,[11] ginkgolides and bilobalide exhibit insect deterrent or insecticidal activity against the fall webworm (*H. Cunea,* 0.31–1.25 mg/mL),[12a] codling moth (*C. pomonella,* 0.1 mg/mL),[12b] brown rice planthopper (*N. lugens,* 0.17–0.26 ng/female) and others.[12] Ginkgo leaves have long been used as bookmarks to protect against page-eating insects like silverfish and booklice.[16b] The insecticidal activity of *Ginkgo biloba* leaves, roots and stems may have provided advantage against predation to preserve the lineage of the early Paleocene species *G. adiantoides*.[13] Benign effects of bilobalide in

humans—in contrast to ginkgolides[14]—commend it as a potentially safe insecticide. The seemingly disparate applications of bilobalide in mammals and in insects derive from activity at homologous ion channels: RDL (**r**esistance to **d**ie**l**drin) receptors in insects and $GABA_A$ (*gamma*-amino butyric acid A) receptors in mammals (Figure 1b).

Bilobalide exhibits insecticidal activity through antagonism of RDL receptors: heteropentameric ion channels gated by GABA. These ionotropic receptors mediate fast synaptic transmission in insect nervous systems. As in mature mammalian systems, the current tends to be inhibitory.[15] Antagonism of these inhibitory channels, therefore, causes increase in spontaneous firing and can prove lethal. As a consequence, RDL receptors are common targets of insect-control agents, such as their namesake, dieldrin, a member of the cyclodiene class. An Ala→Ser mutation within the channel[16] reduces sensitivity to GABA receptor antagonists, including picrotoxinin (PXN, the more active component of the mixed substance picrotoxin, PTX), a plant metabolite of similar formula and topography to bilobalide.[17a]

Dieldrin, PXN and bilobalide also antagonize homologous human GABA-gated ion channels or $GABA_A$ receptors ($GABA_A$Rs). Point mutation of channel residues[17b] identified a likely binding site for bilobalide near the same location as dieldrin and PXN[18]: a wide cavity between 2' and 6' residues on the M2 helix in the transmembrane domain (Figure 1c).[19] (−)-**1** and PXN also display similar potency against a major subtype of GABA receptor in the human brain (IC_{50} = 1.2 μM vs. 4.9 μM, $\alpha_1\beta_2\gamma_{2L}$ @ EC_{50} GABA), although they respond differently to diverse positive allosteric modulators.[20]

Both PXN and dieldrin, however, exhibit marked neurotoxicity in mammals. The latter compound, a polychlorinated pentacycle, persists in the environment, transits along the food-chain and causes multiple disorders in humans.[21] In contrast, bilobalide is well-tolerated in mammals at low to moderate doses and breaks down easily near neutral pH (see below). As a result, there is significant interest in the development of bilobalide as an insecticide.[12] Crude or semi-purified *G. biloba* extracts unfortunately contain ginkgolides A-J, which inhibit RDL receptors but also antagonize human platelet aggregating factor (PAF) and are stable to water.

We became interested in **1** due to its similarity to the *Illicium* sesquiterpenes,[22] which hyperexcite mammalian neurons[22b] but display potentially therapeutic phenotypes in mice, such as normalization of amphetamine-induced hyperlocomotion, an antipsychotic effect.[23] We also recognized the opportunity to investigate broader strategies in polyoxygenated carbocycle synthesis gleaned from work on jiadifenolide[22a] and *O*-debenzoyltashironin,[22b] namely the merger of highly oxidized but sterically congested fragments to accelerate synthesis.[24]

Here we describe our efforts to devise a concise synthesis of bilobalide (**1**), a challenge due to its two hallmark features: 1) congestion, both steric and stereogenic, and 2) polyoxygenation. Together, these features give **1** a very high information density (Figure 2, 1.63 mcbits/ $Å^3$), a measure we introduce here that accounts for the volume occupied by chemical information present in a molecule. In contrast to information content (mcbits),[25]

which mostly reflects heavy atom count and stereocenters, information density (mcbits/ Å^3) reflects how that information is packaged. When high levels of stereochemical information are incorporated into small molecular volumes (i.e. contiguous stereocenters), new interactions and modes of reactivity result. In other words, molecules with high information density can have unexpected emergent properties that alter their stability and reactivity.[26] The efficient conversion of low information-density building blocks into high information-density targets is a fundamental aim of total synthesis. This exercise is particularly important in channel-binding ligands of ionotropic receptors, especially terpenoids typified by **1**, where atoms must be restricted to a small volume: **1** is only 260 Å^3. In comparison, the steroid-derived anxiolytic minaxolone,[27] which binds the extracellular region of $GABA_A$ receptors occupies 498 Å^3 and the insecticidal macrolide ivermectin, which binds the outer transmembrane region, occupies 835 Å^3. Compared to similarly-sized natural products pleuromutilin, himbacine and artemisinin, bilobalide possesses the highest information density, primarily due to its oxygen content, stereocenters and small volume. Stereocenters play a major role in the information density of **1**: an achiral constitutional isomer contains only half the information density (0.94 vs. 1.63 mcbits/ Å^3).

Two overarching strategies differentiate this work from the prior[28,29] syntheses: incorporation of targeted carbon oxidation states in starting materials and formation of hindered C—C bonds between these building blocks. The result, realized retrospectively, is a generally positive increase in average information content;[30] each step productively approaches the target complexity.

The execution of the synthesis relied on recursive feedback between several discoveries that we analyze here in detail. First, we provide a full account of the development of a catalytic, enantioselective Zn^{+2}-Reformatsky aldol that overcomes the thermodynamic instability of the first key building block. Second, experimental observations and mechanistic hypotheses rationalize the development of a stereoselective Mukaiyama hydration reaction, a considerable challenge associated with selective diradical (C• + O_2) collapse. Third, computational analysis describes the driving forces behind the unexpected formation of an oxetane acetal. Fourth, details behind a final, deep oxidation of C10 are provided, including analysis of selectivity using computed pKa.

Results and Discussion.

Foundational work by Corey[28] and Crimmins[29] established successful strategies to complete bilobalide and informed our own orthogonal approach.[31] These prior routes established the contiguous, fully substituted centers of bilobalide early in the synthesis via open-shell intermediates. For example, Corey's synthesis installed every carbon atom of bilobalide in the very first step using a base-mediated annulation (Figure 3), proposed to proceed by single electron transfer followed by diradical collapse. Six of the resulting carbon atoms underwent redox manipulation during elaboration to BB. Of the 21 steps required to elaborate this intermediate to the target, 11 were redox manipulations. Similarly, Crimmins' synthesis established all four contiguous, fully substituted carbons early, at step 8 of 17, via a photochemical enone-olefin [2+2] cycloaddition. Bond formation via the enone triplet excited state ($\pi \rightarrow \pi^*$), radical cyclization and subsequent 1,4-diradical[32] collapse reflects

some mechanistic similarity to ynoate annulation. The resulting cyclobutane contains 5 carbons at the incorrect oxidation state, requiring a total of 8 redox manipulations to reach BB.

In both cases, successful construction of the congested BB core can be attributed to the early transition states of radical reactions that minimize steric repulsion. A more concise synthesis might be achieved if radical reactivity were retained but oxidation patterns of BB were incorporated from the out-set. The pseudosymmetry of the bilobalide bis-lactone suggested a symmetric 1,5-diester starting material that could incorporate many oxidation states and might undergo radical annulation by a 3-carbon fragment with a pendant *tert*-butyl group (see Figure 3 and 4). The C10 hydroxyl of BB, however, proved hard to incorporate into starting material or early intermediates (Figure 4). Therefore, our strategy also hinged on installation of the single hydroxyl late in the synthesis. This late stage oxidation, while simplifying overall, presented an inherent risk due to the topolography of the BB ring system.

The concave core of BB prevents easy access to either hydrogen of lactone D (the 'inner' lactone) in the presence of lactone A (the 'outer' lactone) (Figure 5). Instead, H_k is buried deep within the 'bowl' shape of bilobalide and H_i is occluded by the bulky *t*-Bu group. While retrosynthetically simplifying, this 'deep' oxidation strategy pushed a tremendous amount of risk to the endgame. If the route, however, were accomplished in the projected eight step sequence, a robust supply of *des*-hydroxybilobalide (**2**) would be available for experimentation, mitigating some risk.

We also hypothesized that *des*-hydroxybilobalide (**2**) might form spontaneously from its dihydrate—an aldehyde triacid—and could be a useful thermodynamic sink to target (Figure 3).[85a] Dihydrate **3** could then arise from hydration, alkylation and subsequent global condensation of cyclopentene **4**. The hindered tertiary alcohol of **3**, flanked by two quaternary carbons, would be generated from the corresponding alkene using a Mukaiyama hydration. We previously proposed[33,34] that this base-metal catalyzed radical hydration proceeds via an outer-sphere, metal-hydride atom transfer (MHAT) elementary step, and reasoned that this mechanism would tolerate the extreme steric hindrance of **4** (Figure 3), whereas an inner-sphere coordinative mechanism would fail. Simplified cyclopentene **4** turned out to be merely conceptual; the actual intermediate (**5**) ended up very different.

Initial attempts to forge the key C—C bond between symmetric anion of diester **6** and **7** via aldol reaction were met with failure (Table 1). No product was observed upon addition of **7** to alkali enolates of **6** at cryogenic temperatures. Trace product was observed under equilibrating, basic conditions (entry 3)[35], but attempts to trap the product alcohol through alkylation, acylation or silylation were unsuccessful. These data indicated that the reaction equilibrium lay in favor of **6**, an observation that was subsequently corroborated by the facile retro-aldol reaction of **8** under basic conditions to give **6** and **7** (entry 5).

Instead, we anticipated that vinyl anion addition to the aldehyde would be irreversible (Figure 6) from adduct ***iso*-8**. To test this hypothesis we sought vinyl bromide ***iso*-9**. Surprisingly, Wittig reaction between bromo ylide **10** and β-ketoester **11** resulted in

formation of allylic bromide **9**, through what first seemed to be olefin isomerization (Figure 6). The symmetry of the diester, however, prevented differentiation of H versus Br migration, so a ^{13}C-labelled analogue of **11** (**^{13}C-11**) was synthesized. Following olefination, the ^{13}C labelled position bore the bromide (**^{13}C-9**), indicating migration of the bromide from the ylide to the β-ketoester (**^{13}C-11→^{13}C-12**), followed by olefination. The unexpected α-bromoester might be used in a cryogenic Reformatsky reaction that could promote stabilization of the aldol intermediate through metal chelation between a strongly-bound Zn^{+2} or Sm^{+3} alkoxide and the neighboring benzyl ester.[36,37] Low temperature acidic quench could then prevent retro-aldol.

Initial attempts at a Reformatsky reaction with Zn^0 or In^0 led only to the recovery of starting material or protodehalogenation. After extensive screening, SmI_2 proved to be the ideal reductant,[36,37] affording aldol product **8** in a 15:1 ratio over diastereomer **13** (Figure 7, entry 1 and top HPLC trace). The reaction was reliably scaled to 51 mmol in a single pass using 1 L of a 0.1 M THF solution of SmI_2 (MilliporeSigma). This SmI_2-mediated Reformatsky reaction was utilized for early scale-up campaigns and route scouting, however an asymmetric synthesis of (−)-BB necessitated the development of an enantioselective Reformatsky reaction.

Early trials focused on induction of asymmetry through the use of chiral ligands with SmI_2. Although the work of Proctor[38] led us to test chiral diamines, amino alcohols and cinchona alkaloids, addition of these ligands shut down SmI_2 reactivity or led to unproductive protodehalogenation of **9**. Chiral auxiliaries were unsuccessful due to poor stability of intermediates.

Use of alternative metals to effect the Reformatsky reaction initially fell flat; Zn^0 and In^0 failed to generate product, whereas Cr^{+3} or Cr^{+2}/Ni^{+2} salts led to messy reactions that were poorly diastereoselective. Diethylzinc (Et_2Zn), however, resulted in clean reactions when run at −40 °C, yielding an equimolar mixture of *syn*- and *anti*-aldol diastereomers, **8** and **13** (entry 5). The undesired *anti* diastereomer could not be carried forward to BB due to formation of unproductive diastereomers in subsequent steps. Precedent for the successful use of chiral ligands[39,40] with Zn^0 and Zn^{+2} provided a foundation[41] for experimentation,[42,43,44] however an extensive literature search indicated a paucity of cases in which Reformatsky reactions with aldehydes are rendered both enantio- and diastereoselective[45] using Et_2Zn[46] Most relevant methods involved primary α-haloesters,[47,48] resulting in the formation of single stereocenters.[49,50] This methodological gap provided an opportunity to discover new reactivity.

To this end, a number of easily accessible chiral ligands were screened in combination with Et_2Zn in search of a reaction manifold that would allow for construction of two stereocenters in a single step, and in an enantio- and diastereoselective manner. Optimization data is provided in Figure 7. Unfortunately, many X-type ligands that are commonly employed in Et_2Zn-mediated Reformatsky reactions were unsuccessful in our system, giving either protodehalogenated starting material or complex product mixtures. The first positive results came from the use of L-type ligands including nicotine, and sparteine, and some cinchona alkaloids which generated product, albeit in low dr and *ee* (entries 8-10). Fortunately,

combination of Et_2Zn with BOX or PyBOX ligands led to product cleanly and in high conversion. Each ligand resulted in varying diastereomeric ratios, but often in moderate to excellent enantioselectivities. Notably, temperature significantly influenced background, racemic reaction rate: at −78 °C in the absence of ligand, reaction mediated by Et_2Zn alone was sluggish. The racemic reaction did not compete with the ligand-catalyzed pathway until temperatures reached −40 °C. Use of indabox ligand (−)-**A** at −78 °C gave the best results with a dr of 2.3:1 in favor of **8**, and an excellent *ee* of 94% in favor of the enantiomer corresponding to *nat*-**1**. Other ligands favored the undesired diastereomer **13** but with comparable enantioselectivity. The reaction utilizing indabox ligand (−)-**A** could be rendered catalytic (10 mol%) and was scalable to 51 mmol with careful control of temperature.

From the pseudosymmetric enolate of **9**, two modes of reactivity could feasibly produce alcohols **8** and **13**: 1) formation of an allyl zinc reagent followed by aldehyde addition via allyl-metal reactivity, or 2) via the anticipated Reformatsky-type zinc-enolate addition. ^{13}C-labelled bromide **^{13}C-9** differentiated these pathways in its reaction with diethylzinc and aldehyde **7**, leading to formation of secondary alcohol **^{13}C-8** and **^{13}C-13** (2.3:1.0 dr) as single regioisomers, a result of enolate—not allyl zinc—addition. Despite the low dr, successful formation of this key carbon-carbon bond provided evidence that such an enantioselective, diastereoselective Reformatsky aldol could be rendered catalytic in ligand.

Further studies are underway to understand if a vinylogous diester is necessary for diastereoselectivity and high levels of ee or if simpler secondary α-bromo esters can be used in this general reaction manifold. To the best of our knowledge, this represents the first example of a diastereo- and enantioselective Reformatsky reaction between a zinc enolate and an aldehyde.

Access to **8** set the stage for a 5-*exo*-trig Giese addition via an sp^2-hybridized radical, which we anticipated to be kinetically more reactive than the lower-energy ketyl radical (see Figure 4). Whereas ambient temperature cyclizations proved unsuccessful, elevated temperatures employing standard conditions (1.5 equiv Bu_3SnH, 0.1 equiv AIBN, 85 °C) afforded the cyclopentene as a single diastereomer. The reaction likely proceeds through the transition state of intermediate **15** (Figure 8) to minimize $A^{1,3}$ strain of the β,β-disubstituted enoate and alleviate $A^{1,2}$ strain (see **16**) between the dimethyl acetal and the benzyl ester. Attempts to install C10 oxidation at this stage were also unsuccessful;[51] instead, radical chain propagation by Sn-H atom transfer proved efficient. As an aid to bulk preparation, the desired product could be crystallized from the crude reaction mixture with hot pentanes, obviating the need for large-scale chromatography. One representative run produced 8.1 grams of high purity **14** (>99% *ee* according to chiral SFC analysis).

Formation of the triad of adjacent fully substituted carbon atoms at C3 (*t*-butyl), C8 and C9 entailed Markovnikov hydration of **14** (Figure 9). In a prior synthesis of BB, this transformation proved challenging and required a multi-step sequence including olefin dihydroxylation (OsO_4, pyridine) and selective mono-deoxygenation (1. methyl oxalyl chloride, *i*-Pr_2NEt; 2. AIBN, *n*-Bu_3SnH). Notably, osmium tetroxide dihydroxylation tolerates extreme steric hindrance[52] due to its ‘outer-sphere’ [3+2] cycloaddition mechanism,[53] whereas coordinative ‘inner-sphere’ reactions of hindered alkenes can suffer

very slow rates.[54] Inspired by the steric tolerance of outer-sphere elementary steps, we explored hydration under Drago–Mukaiyama conditions.[34,55] These base-metal catalyzed reactions have garnered significant attention due to their 'mild' conditions, Markovnikov selectivity and ability to tolerate sterically demanding systems. Their extensive use across unique, challenging chemotypes embodies what we call high 'chemofidelity': reliable reactivity, independent of molecular context.[56] Success here relies on the 'outer-sphere' nature of the MHAT mechanism, since the most hindered carbon center does not require a bonding interaction in the transition state, but instead is converted directly to a carbon centered radical.

Unfortunately, the use of standard Mukaiyama hydration conditions produced a near equal mixture of diastereomers and unexpected byproduct **19**, which lacked the *tert*-butyl group (Figure 9). The low diastereoselectivity reflected capture of the open-shell carbon with $^3O_2$, and the byproduct resulted from either Wieland (radical) or Criegee (cationic) fragmentation.[57] Either way, we expected that a decrease in the concentration of intermediate peroxide would minimize **19**. A seminal mechanistic study by Nishinaga et al. on the mechanism of Drago's cobalt salen-catalyzed hydration reported rate acceleration by the addition of triphenylphosphine (10-fold relative to cobalt), which was interpreted to result from the reduction of an intermediate cobalt-peroxide.[58] The hydration of **14** catalyzed by $Co(acac)_2$, however, did not benefit from the addition of triphenylphosphine (PPh_3). Instead, no hydration occurred until all PPh_3 had been oxidized to triphenylphosphine oxide, at which point the same poor reaction mixture resulted! As a result, a series of cobalt, manganese and iron catalysts—shown by Mukaiyama to catalyze the hydrofunctionalization of alkenes—were screened for performance in the presence of PPh_3. $Mn(dpm)_3$ proved optimal but sensitive: PPh_3 allowed catalysis and completely suppressed the formation of **19**, yet its omission led to **19** exclusively. The equivalent reaction rate **14** in the presence of absence of PPh_3 suggested that it did not react with any kinetically relevant species in the Mn-catalyzed reaction. In contrast, PPh_3 shut down the productive reaction pathway of cobalt. Additionally, a variety of Mn, Fe and Co β-diketonate complexes showed no variation in diastereoselectivity, reflecting the outer-sphere MHAT mechanism and capture of dioxygen by a carbon radical.

This discouraging selectivity exposed the inherent limitation of MHAT reactions: substrate dependent stereoselectivity in almost all cases.[59] Solvent screens were possible using cobalt catalysis,[60] but Mn and Fe catalysts typically required an alcoholic solvent to function. Our lab found that these catalysts required alcohol because the standard reductant, $PhSiH_3$, performed poorly compared to its mono-alcoholysis product, *iso*-propoxy(phenyl)silane, a highly efficient reductant that functions in numerous solvents.[61] This reductant allowed an extensive solvent and temperature screen, which to date, had not been reported. It was not clear, however, that solvent choice would increase the stereoselectivity of carbon radical capture by O_2.

To our surprise, solvent played a significant role in stereoselectivity and correlated roughly to Lewis basicity. Ethereal solvent favored the undesired diastereomer **18**, which lactonized due to proximity of the southern benzyl ester. As solvent polarity decreased, the reaction increasingly favored diastereomer **17**. Methylcyclohexane proved to be the optimal solvent

and afforded **17** as the major diastereomer, isolable in 67% yield. These data contrast a recent paper from the Woerpel group that demonstrated small effects of solvent on dr (85:15→97:3), the benefits of which were mitigated by decreases in yield (60→29%). In this case, stereoselectivity was explained by a chair versus twist boat, Fürst–Plattner-like model and required a six-membered ring (Figure 10). Solvent-based stereochemical reversal of five-membered ring hydration (**14→17**), however, is hard to explain with this model. Instead, stereoselectivity might be explained by an internal hydrogen bond between the C6 secondary alcohol and the C5 ester (Figure 10) that is strengthened in conformation **20**. Nonpolar solvents like methylcyclohexane could increasingly favor this interaction, whereas hydrogen bond acceptors like ethers could disrupt it.[62]

These effects highlight the inherent substrate dependent diastereoselectivity in the Mukaiyama hydration, and emphasize how solvent effects can perturb the conformational equilibria of pyramidalized radicals. This represents the first example of a solvent dependence dictating the stereoselectivity of the Mukaiyama hydration, made possible by *iso*-propoxy-(phenyl)silane.

Only a single substitution of the cyclopentane now remained to reach subtarget **3** (Figure 3): stereoselective formation of the C5-C1 bond to form the butyrolactone. Although acylation of the C6 secondary alcohol was achieved with EDCI/ bromoacetic acid, cyclization of **22** to **24** under basic conditions was completely outcompeted by E_1cB elimination to **23**. Attempts to choreograph lactone formation earlier, prior to Mukaiyama hydration, also proved unsuccessful and **25** yielded elimination product **26**, instead of **27**. A number of attempts were made at direct alkylation of **14** by a two-carbon unit via Frater–Seebach alkylation[63,64] with methyl bromoacetate. However, treatment of the alkoxy ester **14** with two equivalents of strong base still led to elimination, leaving the question of stereoselectivity open-ended.

To prevent E_1cB elimination and probe substrate control over the stereoselectivity of C—C bond formation, alcohol **14** was oxidized to β-ketoester **28** (IBX in DMSO). A variety of electrophiles proved incapable of reacting with the extremely hindered carbon C5. *O*-acylation occurred to deliver enol bromoacetate **29**, but radical cyclization to **30** did not. As a result of the congested steric environment, we explored sphybridized electrophiles, including Waser's reagent (TMS-EBX).[65] This isolable alkyne electrophile desilylates with TBAF to deliver the highly reactive parent compound ethynyl benziodoxolone (EBX), which has been isolated recently as its acetonitrile complex.[66] Together, its electrophilicity and small size allowed bond formation at C5 where many other reagents failed. To our frustration, however, the (*R*)-configuration **31** predominated from cyclopentanone **28** (Figure 11).[67]

To reverse this stereoselectivity, we pursued formation of the BB bis-lactone earlier than planned (**17→34→35**, Figure 12), which we thought might direct the delivery of EBX to the correct *Re*-face, at that point a convex surface, of the BB partial ring system. To our surprise, attempted global deprotection of the bis-ester acetal **17** with *para*-toluenesulfonic acid delivered an extremely unreactive oxetane acetal as a 1:3 mixture of diastereomers **36** and **37**, both resistant to epimerization.

The oxetane acetal motif is rare and represented by only a handful of examples in the literature. For example, the human derived platelet aggregation factor thromboxane A2 (TXA_2)[68] contains a cyclic oxetane acetal, but degrades with a half-life of 32 s at 37 °C in pH 7.4 Krebs media. Its instability complicates isolation and requires storage in basic methanol or as the alkali metal salt; the free acid decomposes within hours via oxetane ring opening. This instability is not surprising given the strain energy of oxetanes (E_{strain} ~ 25 kcal/mol),[69] similar to epoxides (27),[69] cyclobutanes (26) and cyclopropanes (28), but substantially less stable than tetrahydrofurans (6 kcal/mol). The oxetane acetals of both TXA_2 and dehydrated rhamnopyranoses[70] are formed under basic conditions as a result of acid lability. In addition to TXA_2, two other naturally-occurring oxetane acetals have been isolated: oxetanocin A (a hemiaminal)[71] and maoecrystal I;[72] however neither compound appears to possess a facile path to decomposition via oxetane ring-opening.

In contrast, oxetanes **36** and **37**, we thought, could easily open via formation of a methyl oxocarbenium ion, which could then either hydrolyze or demethylate. Its stability, however, might reflect a general feature of the bilobalide scaffold. A similar, albeit internal, acetal was reported recently as an intermediate in an approach towards the synthesis of bilobalide and survived a strongly acidic, oxidizing step (CrO_3, H_2SO_4, acetone).[73] Our attempts to deprotect or epimerize the oxetane acetals **36** and **37** led to recovery of starting material, and caused us to investigate their unusual persistence.

Steric congestion imparted by the multiple quaternary carbons and *tert*-butyl substituent could be considered the defining idiosyncrasy of the bilobalide ring system, and one which might reasonably play a role in oxetane persistence. Such an effect is well precedented in the synthesis and study of tetra-hedranes, including tetra-*tert*-butyl tetrahedrane (***t*-Bu$_4$T**), which despite its strain energy (E_{strain} ~ 130 kcal/mol) melts at 135 °C.[74] This requirement of steric congestion was attributed to the ‘corset effect’ whereby bond scission increases repulsive steric interaction in the transition state, leading to a high energy barrier. It was not clear whether the unusual stability of **36** and **37**, however, derived from substrate stabilization, transition state destabilization or product destabilization.

Density functional theory (DFT) calculations probed whether the unusual stability of the oxetane acetal was kinetic or thermodynamic in origin. Whereas a significant barrier to protolytic ring-opening could not be found, hydrolysis was calculated to be thermodynamically uphill for **36** and **37** in DMSO, THF and water (Figure 13), despite the expected release of considerable ring strain. Replacement of the *tert*-butyl group with progressively smaller alkyl substituents revealed its key role in tipping the thermodynamic balance against the hydrolyzed free aldehyde **39a–d**. With an isopropyl substituent, the proximal ester group was free to assume a conformation that avoided clash with the distal ester group. In contrast, a *tert*-butyl substituent in the same position forced the two ester moieties into close proximity with each other, creating repulsion that destabilized ring-opened form **39a** (Figure 13).

These effects were analogous to Maier’s corset effect: strain-release through small ring-opening was offset by destabilizing repulsion between substituents (Figure 14). An alternative hypothesis suggested by calculated Intrinsic Reaction Coordinates (IRCs)

involved formation of stable oxocarbenium intermediates **40** or **41**, which might persist in acidic media but revert to oxetane on basic work-up. This hypothesis was probed by monitoring **36** in situ. In fact, the oxetane acetals themselves were remarkably persistent, even in concentrated, strong acid. As shown in Figure 15, both **36** and later intermediate **48** were stored in 1.5 M DCl (1:1 THF-d_8/ D_2O) for over 24 h with no change in their ^1H NMR spectra. The lack of epimerization, oxocarbenium formation or hydrolysis indicated either a high kinetic stability or rapid internal return of a thermodynamically less stable oxocarbenium **40** or **41**.

The oxetane acetal motif proved more than an idiosyncrasy: its deformation of the bilobalide ring system ultimately allowed for completion of the synthesis, with one caveat. Only *endo*-methoxy oxetane **36**, the minor isomer (20% isolated, using TsOH•H_2O), could be advanced to bilobalide.

We had hoped that the oxetane would effectively shield the enolate *Si*-face from attack to produce alkyne **42**. Unfortunately, treatment of *exo*-methoxy oxetane **37** with IBX followed by Waser's reagent only afforded rearrangement product **43**, possibly derived from the desired, albeit unstable isomer **42**. Minor isomer **36**, on the other hand, could be oxidized to **44** and alkynylated to **45** in good yield (≥61%) and as a single diastereomer.

After IBX-mediated oxidation and TMS-EBX-mediated alkynylation, the synthesis required return to the alcohol oxidation state. This task was complicated by the instability of β-ketoester **45**, which decomposed on silica or prolonged standing, and the tendency of the ketone to undergo reduction to **46** from the *Si*-face of C6 by hydridic reagents, as confirmed by X-ray crystallography (**47** X-ray). Inspired by a proposed directed reduction in Evans' synthesis of cytovaricin,[75] we explored SmI_2, which had been proposed to favor stereoisomers that could accommodate a chelated organosamarium(III) intermediate. In this case, chelation to the Lewis basic oxetane acetal might direct the reduction. In accordance with Evans' model, stereoisomer **5** was formed with high (>20:1) selectivity (see **5**, X-ray). This key sub-target (see Figure 3) contained all the carbon-carbon bonds of **1** and required seemingly simple hydration/dehydration chemistry to complete the target, yet derived from the minor diastereomer (**36**) of oxetane (Figure 16).

Attempts to reverse the stereoselectivity of oxetane acetal formation (**17→36/37**) were initially unsuccessful. Neither solvents, simple Brønsted acids or Lewis acids led to an excess of **36**. However, we observed that certain chiral phosphoric acids afforded a modest dr of 1.7 : 1.0 in favor of **36**. Given the cost of these catalysts and the low selectivity, such a solution seemed impractical. However, when working with racemic material (i.e. *rac*-**17**), we observed by chiral supercritical fluid chromatography (SFC) that each diastereomer was enriched in opposing enantiomers: chiral phosphoric acid (−)-**A** in a mixture of THF and H_2O led to *exo*-oxetane **37** in 69:31 er and *endo*-oxetane **36** in 39:61 er. In other words, each enantiomer of *rac*-**17** reacted with catalyst (−)-**A** to give opposing diastereomeric ratios (see Figure 17): (−)-**17** favored *exo*-isomer **37** (29:21) and (+)-**17** favored *endo*-isomer **36** (39:11).

These observations suggested that a parallel kinetic resolution had occurred during oxetane acetal formation. [76] This effect is consistent with enantio-differentiation of prochiral acetals by chiral phosphoric acids reported by the List group.[77] The same report noted that a partial parallel kinetic resolution occurred with a substrate bearing a tertiary alcohol.

In collaboration with the Scripps Automated Synthesis Facility, we developed a two-dimensional (2D) liquid chromatography (LC) / chiral SFC separation to directly probe effects of solvent, temperature and catalyst structure on the efficiency of PKR (Figure 17). Consequently, crude racemic reaction mixtures divulged their selectivity profile (dr, er) without purification.[78] Pure, internal 'slices' of each 1st dimension (LC) peak were internally directed to a chiral SFC system that separated the enantiomers of each diastereomer, quickly providing the user with ratios of all four stereoisomers of interest. A similar 2D method was developed during optimization of the Reformatsky reaction.

Multiplication of dr by er of each diastereomer derived from *rac*-**17** delivered the ratio of *endo* and *exo* diastereomers for each enantiomer of **17**. Reactions of enantiopure (+)-**17** produced diastereoselectivities that corresponded well to those derived from 2D analysis and deconvolution. This method allowed us to work in parallel: we optimized the diastereoselectivity for **17→36** while the enantioselective Reformatsky (**9→8**) was under development and (+)-**17** was not readily available.

The data in Figure 17 indicated that lower temperature, non-aqueous solvent (cyclohexane) and phenanthryl substituents on the chiral acid provided the highest selectivity (5.3 : 1.0) for *endo*-isomer (+)-**36** from (+)-**17**, whereas the *exo*-isomer (-−)-**37** was produced from (−)-**17** with 1.0 : 3.2 selectivity. Diastereoselectivity combined with product enantioenrichment allowed prediction of dr using a one enantiomer of **17**. This singular antipode was available from the catalytic enantioselective Reformatsky discovered in step two of the synthesis, combined with purification by crystallization, which enriched enantiomeric excess to >99% *ee*. In the event, (+)-**17** was converted with 5.3 : 1.0 selectivity to (+)-**36** under optimal conditions.

The alkyne subunit had been installed as a surrogate for an acetate appendage, however its hydration and oxidation proved non-trivial. We planned to oxidize the alkyne using standard conditions (Figure 18).[79] Unfortunately, only hydroboration (BH_3•THF) and iterative oxidation (1. $Na_2B_2O_3$; 2. TEMPO, PIDA) successfully generated the target lactone **48**, and this only in 23% yield. The yields severely diminished when the reaction was run on scales larger than 0.1 mmol. An alternative solution was inspired by a report by Julia that alkyne oxidation could be carried out directly using LiOO*t*-Bu/LiHMDS by way of an intermediate lithium ynolate.[80] Application of these conditions led to recovered starting material and a trace amount of the TMS-protected alkyne, which implicated at least partial deprotonation of **5**. We hypothesized that the alkynyl lithium could not efficiently coordinate LiOO*t*Bu, whereas a more Lewis acidic substrate might. Ultimately, we found that the alkynyl lithium intermediate reacted efficiently with trimethylborate, $B(OMe)_3$ to generate a transient alkynylborate anion. Only *m*-CPBA effected oxidation to the lactone, presumably by protonation of one methoxide ligand and capture of the trivalent boron by the peroxybenzoate,[81] as suggested by early work on alkoxyboronates by Brown.[82] Migration of

the alkyne into the adjacent O—O σ* orbital would generate an intermediate boron ynolate, which could cyclize to lactone **48** via several pathways. Protonation with benzoic acid or perbenzoic acid could generate a ketene or, if captured, a mixed anhydride. Alternatively, the boron ynolate might be stable until addition of aqueous NH_4Cl. No byproducts were isolated that provided insight into mechanistic details, but an upcoming report from the Ohtawa lab seeks to shed light on this question.[83]

The question of whether the bilobalide ring system represented a thermodynamic sink and whether the unusually stable oxetane would deprotect under suitable conditions now lay before us. Impatience to answer this question and attempt the final, deep oxidation (‘inner’ versus ‘outer,’ lactone D versus A) led to a mechanistic morass that would consume over nine-months of research.

Because oxetane **48** proved stable to Brønsted acid, a dealkylating Lewis acid, BBr_3 (>10 equivalents), was added to **48** to decompose both the methoxy acetal and the benzyl esters. To our surprise, *des*-hydroxybilobalide was produced on the first attempt, albeit in apparent low (*ca*. 30%) yield. This result dispelled the uncertainty of whether the bilobalide dilactone acetal would serve as a thermodynamic sink to which the acyclic carboxylates might funnel. Flush with success, the single milligram of crude **2** was subjected to conditions that might hydroxylate either lactone, with the hope that luck was now on our side. Treatment of crude **2** with NaHMDS, $P(OEt)_3$, and O_2 delivered a new product by TLC (with prolonged heating for visualization, see below) and ^1H NMR of material recovered after workup showed unambiguous peaks of bilobalide as the major product (see Figure 19a).[84]

This result was extraordinary given the apparent inaccessibility of the C10 protons. Our delight was fleeting: the reaction has never been reproduced even to this day.

Repeated attempts to effect the oxidation of **2** to **1** under the original conditions by the same or different personnel either returned starting material or produced the undesired (but expected) isomer, designated *neo*-bilobalide (**49**, Figure 19b), a result of oxidizing the more accessible ‘outer’ lactone. Although the adage ‘garbage-in, garbage-out’ proved partly true, a reproducible procedure for the final oxidation may never have been discovered without this crucial reconnaissance. The process of invention now became archaeology: what had happened the first time?

The base lability of bilobalide provided the first evidence for a complex mechanism of oxidation. Its instability has led to many optimizations of extraction and purification from *G. biloba* leaves.[85] At pH 3, the trilactone fraction (ginkgolides and bilobalide) appears stable, but at pH 6.5 mono-lactone saponification of ginkgolide B occurs. Strongly basic (pH 10.4) aqueous washes of crude *G. biloba* extract removes BB and ginkgolide C from the organic phase. However, acidification of the aqueous phase with 1N HCl, followed by reextraction with EtOAc only leads to the recovery of ginkgolide C whereas BB decomposes and cannot be recovered.[85a] BB has been found to irreversibly decompose at pH values above 7,[86] likely through irreversible lactone opening.[87] To date, these decomposition byproducts have not been characterized and the pathway for irreversible BB decomposition remains unknown.

This information is important for both isolation and pharmacokinetics: BB degrades in rat heparinized plasma ($k = 0.5465\ h^{-1}$) and even in pH 7.4 buffer ($k = 0.1868\ h^{-1}$).[88]

The base instability of bilobalide might derive from its rapid rearrangement to *iso*-bilobalide. A similar rearrangement had been observed by Weinges and co-workers upon treatment of bilobalide with acetic anhydride and pyridine, which delivered diacetoxy-*iso*-bilobalide.[89] However, we found rearrangement occurred simply upon treatment with base (Figure 20a). The C8 tertiary alcohol is positioned within the Burgi–Dunitz angle of lactone A, which is rendered more electrophilic by lone pair hyperconjugation, and its translactonization pulls the *tert*-butyl away from C10. For example, addition of 1 equivalent of the weak base DBU to a $CDCl_3$ solution of **1** or **2** effects quantitative conversion to translactonized products **51** or **52**. Similarly, we found that treatment of **2** at −78 °C with 1 equivalent of the strong base KHMDS—the same base used for attempted lactone hydroxylation—followed by 1 equivalent of 1M methanolic HCl quantitatively forms ***iso*-2**, which is unstable in acid, difficult to isolate and slowly reverts to **2**. Since rearrangement to the *iso*-bilobalide skeleton (***iso*-2**) occurred first, it clearly played a role in the irreproducible deep oxidation.

The original, successful oxidation (**2** to **1**) must have occurred via the base-induced *iso*-bilobalide rearrangement, given its facility in the presence of base. This hypothesis benefited from molecular models that indicated the *iso*-bilobalide skeleton increased access to C10 of the 'inner' lactone (see Figure 20b). However, if rearrangement alone were necessary, any successful oxidation should deliver **1**. In reality, any conditions for α-hydroxylation including KHMDS/ Davis' oxaziridine (**50**) yielded exclusively the C1-oxidized isomer **49** via oxidation of the outer lactone.

Recall that global deprotection of **48** was carried out using BBr_3. This procedure reliably provided low yields of **2**, but when oxidation to **1** failed repeatedly (with crude or purified material), we took the opportunity to improve the deprotection. To our surprise, **48** was completely stable to 3 M HCl at 80 °C for over 12 h, reflecting the remarkable 'corset' fortification of the oxetane acetal (see Figure 15). However, hydrogenolysis of the benzyl esters (Figure 21) significantly enhanced the reactivity of the oxetane: now 3 M HCl over 12 h produced **2** cleanly, which supports the equilibrium 'corset' effect proposed above.

Perhaps a boron impurity led to formation of **1** by capturing the opened isomer as **54**, the borate of ***iso*-2**. Unfortunately, addition of boron Lewis acids—BBr_3, $B(OMe)_2$, $EtB(OH)_2$, etc.—either prevented reaction or had no effect. However, attempts to mimic the borylated *iso*-bilobalide intermediate using a *tert*-butyl-dimethylsilyl (TBS) group (**55**) met with modest success: for the first time in nine months, bilobalide was observed in the crude ^1H NMR, albeit as the minor isomer (1:16) versus *neo*-bilobalide.

A major difference between silicon and boron is the effect of valence bonding on electron delocalization. In this case, a trivalent boron (e.g. **54**) might acidify the α-protons (i.e. stabilize the corresponding enolate) via B—O π-bonding[90] and delocalization of the lactone π-system into an adjacent C-O σ* orbital, more so than the corresponding Si—O substituent (e.g. **55**). Analogous delocalization is common in glycosides and reflected by changes in

bond lengths to the anomeric carbon.[91] In the case of chloro-glycosides, the axial conformer has a 0.62 Å shorter C—O bond and a 0.105 Å longer C—Cl bond than its equatorial isomer (see Supporting Information), as a result of oxygen lone-pair delocalization into the antiperiplanar antibonding orbital of the adjacent carbon halogen bond..[92] In the case of an α-hydroxy lactone, this lone pair delocalization into the anomeric antibonding orbital could decrease the lone pair donation into the adjacent carbonyl, making it more electron deficient. [93] In turn, this deficiency should make the carbonyl more ketone-like and result in acidification of the α-protons.

We were unable to isolate a boric acid or boric ester derivative of *des*-hydroxy-isobilobalide ***iso*-2**, consistent with the absence of borylated γ-hydroxy lactones in the literature, so we turned to an electronically equivalent group. Whereas silylated γ-hydroxy lactone **55** would not benefit from the same acidification of a borylated γ-hydroxy lactone (cf. TBSOH pKa = 15.36 versus $B(OH)_3$ pKa = 9.24),[94] a benzoyl group (BzOH pKa = 4.20) might prove suitable. This derivative (**56**) was synthesized from **2** with DMAP, EDCI and benzoic acid (see Figure 22a/b). Drawing analogy to haloglycosides (see above), we compared the bond lengths at the anomeric carbon of **56** to other substituted γ-hydroxy lactones (see Supporting Information S38) and observed a similar trend. Electron withdrawing groups adjacent to the ethereal oxygen of γ-hydroxy lactones cause a shortening of the anomeric C—O bond and a lengthening of the lactone C—O bond (see Figure 22c). These data derived from crystal structures, and DFT calculations found similar trends (Figure 22d). Compared to 4-hydroxy-γ-lactone (pKa = 22) and its *tert*-butyldimethylsilyl ether (21.8), the borate (18.6), acetate (17.3) and benzoate (17.8) were significantly more acidic and exhibited bond length changes consistent with O lone pair delocalization into the σ* orbital of the substituent; overall this decrease in the C—O π character might acidify the C-10 α-protons.

In the event, subjection of benzoylated intermediate **56** to KHMDS and Davis oxaziridine yielded, to our immense relief, bilobalide (**1**) in 91:9 preference to its isomer, *neo*-bilobalide (**49**). This acidification of α-protons through the anomeric effect appeared to be unique and warranted further investigation. Acidification of the α-protons might open two pathways to C10 oxidation: 1) direct deprotonation of the C10 position (**56•K_D**, Figure 23) or 2) indirect deprotonation via proton exchange with the enolate of the more accessible outer lactone A (**56•K_A**).

Experiment effectively differentiated these pathways. First, we found that deprotonation occurred very quickly: incubation of **56** with base for 60, 30 or 10 minutes did not change conversion to **1**. Second, based on recent reports that Davis' oxaziridine (**50**) does not react with KHMDS at cryogenic temperatures,[95] we probed the possibility of enolate-lactone proton exchange by addition of KHMDS to a mixture of **50** and **56**. The result was a 60:40 mixture of **1:49** (bilobalide : *neo*-bilobalide), revealing that deprotonation occurs at C1 (lactone A, **56•K_A**) followed by an enolate equilibration to C10 in the anomerically-stabilized lactone D (**56•K_D**). Whether this equilibration occurred by intermolecular or intramolecular proton transfer was determined by varying the concentration of **56** at a constant concentration of **50**. A positive correlation between **1:49** and [**56**] revealed an intermolecular exchange: as the rate of productive collisions between substrates increased, the concentration of inner enolate increased.

Consistent with this data, deprotonation at C10 (inner lactone) was calculated to be 4.3 kcal/mol more favorable than deprotonation at C1 (outer lactone), meaning that the inner lactone is about 3 pKa units more acidic. This acidification is primarily due to the anomeric and inductive effects of the pendant ester moiety, which is absent in the outer lactone ring.[96] We suspect that the original, irreproducible oxidation occurred from an *iso*-bilobalide borate (**54**, Figure 21a, 22a) similar to **56**.

All the data taken together indicates that the inner lactone is inaccessible to base for direct deprotonation. Even in the unfolded *iso*-bilobalide analogs (**55**) and (**56**), deprotonation occurs initially from the outer lactone. Fortunately, acidification by the benzoate allows the conjugate base of the outer lactone—*the kinetic acid*—to intermolecularly deprotonate the inner lactone—*the thermodynamic acid.* This funneling of reactivity from an outer to an inner site allows deep oxidation and completion of the target (Figure 24).

Effects on spontaneous $GABA_A$ receptor-mediated synaptic transmission.

Our interest in the synthesis of bilobalide (**1**) stemmed from our hypothesis that the so-called 'neurotropic' sesquiterpenes shared the functional properties of **1** and other prototypical $GABA_A$ receptor antagonists,[97] and therefore may hold similar therapeutic potential. We recently showed that (−)-jiadifenolide and (−)-11-*O*-debenzoyltashironin caused hyperexcitation of neurons,[22b] consistent with a model of excitatory neurite outgrowth. This hypothesis was formulated based on structural overlap between jiadifenolide (J, 239 $Å^3$) and picrotoxinin (PXN, 229 $Å^3$),[97] an overlap shared by bilobalide (BB, 260 $Å^3$) (see Figure 1).[17a] We have begun to annotate similarities and differences between these small, dense sesquiterpenes.

PXN and BB exhibited strong antagonism in functional and binding assays, whereas J reduced GABA-evoked currents about 300X more weakly than PXN and did not displace channel ligand [^{3}H]-BOB; molecular dynamics suggested a binding site for J closer to the intracellular pore.[23] Nevertheless, J caused robust hyperexcitation of neurons at 30 μM.[22b] Whereas PXN and BB shared similar potencies, only PXN was a strong convulsant (CF-1 mice; 3 mg/kg SC). BB was only convulsant at high dose (100-300 mg/kg PO) and J was nonconvulsive (up to 150 mg/kg IP).[23] Nevertheless, intraperitoneally-dosed J reached total brain concentrations of 26 μM (13 μM unbound) and attenuated amphetamine-induced hyperlocomotion, similar to picrotoxin at nonconvulsive dose.[23]

Given the *in vitro* effects on $GABA_A$ receptor-mediated currents by BB and J, we aimed to explore whether BB and J would also affect $GABA_A$ receptor mediated synaptic transmission in *ex vivo* brain slice preparations. The central nucleus of the amygdala (CeA) is highly GABAergic,[98,99,100] thus we compared BB and J directly in acute CeA brain slices from male Wister rats at low concentrations to study their effects on pharmacologically isolated miniature inhibitory postsynaptic current (mIPSC). The brevity of our synthesis also enabled easy access to *ent*-BB (i.e. (+)-bilobalide), which served as a negative control and also allowed us to exclude the possibility that achiral metabolites of BB cause excitatory effects. Remarkably, despite profound differences in potency at recombinant $GABA_A$ receptors, BB and J exhibited very similar effects at 1 μM to reduce mIPSC frequencies and amplitudes (Figures 25a-c, summarized in 25d).

Importantly, these data underline a direct interaction of (−)-jiadifenolide and (−)-bilobalide with native $GABA_A$ receptors and $GABA_A$ receptor-mediated synaptic transmission, further supported by lack of activity of the enantiomer (+)- bilobalide. To the best of our knowledge, these are the first studies to show the effects of bilobalide on action-potential independent mIPSCs. The activity of safe $GABA_AR$ antagonists (−)-jiadifenolide and (−)-bilobalide may indicate translation potential, given the importance of GABAergic transmission in the CeA in fear processing, anxiety, negative emotions and addictive disorders such as alcohol use disorder.[98,101,102] The most surprising finding here may be the large difference in relative potencies of (−)-jiadifenolide and (−)-bilobalide between recombinant $GABA_A$ receptors ($\alpha_{1\text{-}5}\beta_3\gamma_2$) (where jiadifenolide is about 50X lower in potency than bilobalide) and $GABA_A$ receptors in native brain tissue (where jiadifenolide is equipotent to bilobalide). Such a discrepancy may indicate either subtype-selective antagonism or potential mechanistic differences in antagonism at submaximal GABA concentrations (recombinant expression system) versus millimolar GABA concentrations in the synaptic cleft required for mIPSCs. Furthermore, this discrepancy could also arise from using isolated systems (HEK cells) versus brain slices representing a more physiological preparation. In fact, in acute brain slices, the neurons express a variety of different $GABA_A$ receptor subunits and maintain their physiological intracellular signaling and in part their connectivity.

Conclusion.

Chemical synthesis can be viewed as the encoding of information content in a molecular structure. Secondary metabolites tend to encode information differently than other types of complex structures (dendrimers, dyes, drugs) and include a greater fraction of sp^3 hybridized atoms (Fsp^3),[103] high chiral atom content, high heteroatom content and low aromaticity. Total synthesis encodes this complexity by joining together low information content reactants, but aims for greater-than-additive products. Our group (R.M.D, M.A.B, M.O., R.A.S.) is interested in objectively measuring this process and has turned to Böttcher's complexity index (C_m)[25] to formalize intrinsic information content.[104] Böttcher scores assign information content (mcbits) to each non-hydrogen atom, which are added to measure molecular complexity, a comparative index given as C_m. Representative Böttcher indices correspond, in part, to the results of Bertz's graph theory-based $C(\eta,\varepsilon)$ complexity index,[105] yet can be done with pencil and paper, albeit slowly. The Supporting Information for this paper includes a Python script[106] (written by S. F.) that annotates molecules with Böttcher scores using a SMILES string input at a rate of ca. 132,000 compounds per minute, simplifying use of this metric. C_m does not include any aspect of synthetic difficulty, a changing and subjective measure.[107] Its ease and objectivity make C_m an appealing measurement of complexity.

In Figure 26, we view the three syntheses of bilobalide through the lens of C_m changes. Each intermediate was assigned a C_m value and scores were averaged per atom to mitigate the effect of protecting groups, which can carry high information content without contributing to core complexity. After normalizing the C_m scores, all three syntheses started from similar complexity scores, but advanced to the target at different rates and different sacrifices in complexity, reflecting different step counts.

We had qualitatively rationalized our choices in synthesis design as efficient through minimization of redox reactions and sought a Böttcher analysis to quantitatively interrogate this idea. Summation of the raw scores of carbons that have an oxygen atom in bilobalide (C2, 4, 6, 8, 10, 11, 12) revealed three trends: 1) our work began from a higher total score, largely due to initial incorporation of bislactone oxygens in their final oxidation state, and therefore minimized the total oxidative distance to product, significantly lowering necessary operations; 2) the percentage of steps in a synthesis that result in an overall *decrease* in complexity at the carbons of interest was generally consistent across all three syntheses regardless of step count: this work: 25%, Crimmins: 35%, Corey: 27%, therefore future strategies might try to minimize these sacrificial maneuvers; 3) a direct correlation existed between step count and complexity score changes at carbons bearing a heteroatom in a particular synthesis: this work = 10 (83% of 12 total steps), Crimmins = 16 (94% of 17 total steps, *racemic*), and Corey = 20 (83% of 24 total steps, *asymmetric*). The most telling metric of synthetic efficiency here is the total number of times these oxidized carbon atoms change complexity scores throughout the synthesis. Ideally, a carbon atom is introduced in the synthesis at its final value (oxidation state, hybridization, stereochemistry) or undergoes minimal transformations to reach the target score.

Information content is easy to buy; information density is not. The dense packaging of information in natural product space is not unique to bilobalide; in fact, high information density may describe much of natural product space. Bilobalide uniquely fills a biologically-privileged and poorly-explored region of chemical space characterized by unusually information-dense structures. Our synthesis addresses the challenge of encoding dense content through several features: 1) embedding oxygenation, largely of the correct oxidation state, in starting materials; 2) development of a catalytic, asymmetric Reformatsky reaction to merge these starting materials with high enantioselectivity; 3) use of radical reactions that benefit from early transition states to establish sterically congested centers, including 4) a solvent-controlled stereoselective Mukaiyama hydration that tolerates steric bulk via an outer-sphere MHAT elementary step; 5) use of extreme steric repulsion to leverage an unusually stable oxetane acetal in stereoselective C—C bond formation via 6) the sterically small, but highly electrophilic Waser's reagent (TMS-EBX). Finally, the hypothesis that the bilobalide scaffold represented a thermodynamic sink allowed a late-stage, global deprotection to reach penultimate intermediate *des*-hydroxy-bilobalide (**2**). Crucial reconnaissance revealed the potential to effect selective oxidation of the hindered, inner lactone, which was reproducibly executed after significant interrogation and mechanism-based experimentation.

Information dense (high mcbits/ $Å^3$) natural products can be efficiently 'encoded' by incorporation of heteroatoms and oxidation states into starting materials. In principle and in practice,[24] this approach allows a simple, combinatorial route to dense, polyoxygenated libraries. When paired with a macromolecular target, we imagine that oxygenation patterns of bioactive natural products can be altered to uncover simpler paths to oxygenated starting materials yet maintain target affinity.[108,109] Both strategies require close collaboration between chemistry, computation and biology, and for the fields to understand one another with clarity. The push to develop retrosynthetic software superior to original iterations[110]

requires a clear-eyed understanding of how synthesis is actually conceived and executed. Here we have delineated in granular detail the recursive feedback of experimental results into synthetic design. In addition to the provision of 1) tools for $GABA_AR$ biology, 2) code for molecular complexity, 3) methods for catalytic enantioselective synthesis and 4) combined computational/ experimental insight, we hope this work provides a clear illustration of the interplay between synthesis, mechanism and computation in the current era.

Supplementary Material

Refer to Web version on PubMed Central for supplementary material.

ACKNOWLEDGMENT

Support was provided by the National Institutes of Health (R35 GM122606, R.A.S.; P60 AA006420 and AA015566, M.R.), Jiangsu Industrial Technology Research Institute (M.A.B.), the Uehara Memorial Foundation (M. O.) and the National Science Foundation (CHE-1955922, R.A.S; CHE-1764328, K.N.H). Calculations were performed on the Hoffman2 cluster at the University of California, Los Angeles, and the Extreme Science and Engineering Discovery Environment (XSEDE), supported by the National Science Foundation (OCI-1053575). C.C.L. is grateful to the Imperial College Bursary Scheme for funding. We thank Dr. Jason S. Chen and Brittany Sanchez of the Scripps Automated Synthesis Facility for help with separations and analysis. We gratefully acknowledge Brandon Wright, Robert Lusi and Professor Richmond Sarpong for beta-testing the Böttcher score code, and Professor Böttcher for helpful correspondence.

REFERENCES

(1). Seeff L; Bonkovsky HL; Navarro VJ; Wang G Herbal products and the liver: A review of adverse effects and mechanisms. Gastroenterology 2015, 148, 517. [PubMed: 25500423]

(2). https://www.fda.gov/food/dietary-supplements

(3). For modest, positive effects, see: (a) Le Bars PL; Katz MM; Bermann N; Itil TM; Freedman AM; Schatzberg AF A placebo-controlled, double-blind, randomised trial of an extract of Ginkgo biloba for dementia, North American EGb Study Group. JAMA 1997, 278, 1327; [PubMed: 9343463] (b)Herrschaft H; Nacu A; Likhachev S; Sholomov I; Hoerr R; Schlaefke S Ginkgo biloba extract EGb 761® in dementia with neuropsychiatric features: a randomised, placebo-controlled trial to confirm the efficacy and safety of a daily dose of 240 mg. J. Psychiatr. Res 2012, 46, 716; [PubMed: 22459264] (c)Tan MS; Yu JT; Tan CC; Wang HF; Meng XF; Wang C; Jiang T; Zhu XC; Tan L Efficacy and adverse effects of ginkgo biloba for cognitive impairment and dementia: a systematic review and meta-analysis. J. Alzheimers Dis 2015, 43, 589; [PubMed: 25114079] (d)Yuan Q; Wang CW; Shi J; Lin ZX Effects of *Ginkgo biloba* on dementia: An overview of systematic reviews. J. Ethnopharmacol 2017, 195, 1. For no effect, see:(e)Schneider LS; DeKosky ST; Farlow MR; Tariot PN; Hoerr R; Kieser M A randomized, double-blind, placebocontrolled trial of two doses of *Ginkgo biloba* extract in dementia of the Alzheimer's type. Curr Alzheimer Res. 2005, 5, 541;(f)Butler M; Nelson VA; Davila H; Ratner E; Fink HA; Hemmy LS; McCarten JR; Barclay TR; Brasure M; Kane RL Over-the-Counter Supplement Interventions to Prevent Cognitive Decline, Mild Cognitive Impairment, and Clinical Alzheimer-Type Dementia: A Systematic Review. Ann. Intern. Med 2018, 168, 52; [PubMed: 29255909] (g)DeKosky ST; Williamson JD; Fitzpatrick AL; Kronmal RA; Ives DG; Saxton JA; Lopez OL; Burke G; Carlson MC; Fried LP; Kuller LH; Robbins JA; Tracy RP; Woolard NF; Dunn L; Snitz BE; Nahin RL; Furberg CD Ginkgo Evaluation of Memory (GEM) Study Investigators, *Ginkgo biloba* for prevention of dementia: a randomized controlled trial. JAMA 2008, 300, 2253; [PubMed: 19017911] (h)Vellas B; Coley N; Ousset PJ; Berrut G; Dartigues JF; Dubois B; Grandjean H; Pasquier F; Piette F; Robert P; Touchon J; Garnier Mathiex-Fortunet, H.; Andrieu S; GuidAge Study Group. Long-term use of standardised *Ginkgo biloba* extract for the prevention of Alzheimer's disease (GuidAge): a randomised placebo-controlled trial. Lancet Neurol. 2012, 10, 851;(i)Charemboon T; Jaisin K *Ginkgo biloba* for prevention of dementia: a

systematic review and meta-analysis. J. Med. Assoc. Thai 2015, 5, 508;(j)Laws KR; Sweetnam H; Kondel TK Is *Ginkgo biloba* a cognitive enhancer in healthy individuals? A meta-analysis. Hum Psychopharmacol. 2012, 6, 527;(k)For a summary, see: Nguyen T; Alzahrani T Ginkgo Biloba [Updated 2019 Oct 3]. In: StatPearls [Internet]. Treasure Island (FL): StatPearls Publishing; 2019 1-. Available from: https://www.ncbi.nlm.nih.gov/books/NBK541024/

(4). Mei N; Guo X; Ren Z; Kobayashi D; Wada K; Guo L Review of *Ginkgo biloba*-induced toxicity, from experimental studies to human case reports. J. Environ. Sci. Health Part C 2017, 35, 1.

(5). Clarke TC; Black LI; Stussman BJ; Barnes PM; Nahin RL Trends in the use of complementary health approaches among adults: United States, 2002–2012 National health statistics reports 2015, no. 79 Hyattsville, MD: National Center for Health Statistics.

(6). Madgula VL; Avula B; Yu YB; Wang YH; Tchantchou F; Fisher S; Luo Y; Khan IA; Khan SI Intestinal and blood-brain barrier permeability of ginkgolides and bilobalide: in vitro and in vivo approaches. Planta Med. 2010, 76, 599. [PubMed: 19937548]

(7). NTP Technical Report on the Toxicology and carcinogenesis studies of *Ginkgo biloba*extract (CAS No. 90045-36-6) in F344/N rats and B6C3F1/N mice (Gavage studies). Natl. Toxicol. Program Tech. Rep. Ser 2013, 578, 1.

(8). Fernandez F; Morishida W; Zuniga E; Nguyen J; Blank M; Malenka RC; Garner CC Pharmacotherapy for cognitive impairment in a mouse model of Down syndrome. Nature Neurosci. 2007, 10, 411. [PubMed: 17322876]

(9). Kiewert C; Kumar V; Hildmann O; Rueda M; Hartmann J; Naik RS; Klein J Role of GABAergic antagonism in the neuroprotective effects of bilobalide. Brain Res. 2007, 1128, 70. [PubMed: 17134681]

(10). Masiulis S Desai R; Uchanski T; Martin IS; Laverty D; Malinauskas T; Zivanov J; Pardon E; Kotecha A; Steyaert J; Miller KW; Aricescu AR $GABA_A$ receptor signaling mechanisms revealed by structural pharmacology. Nature 2019, 565, 454. [PubMed: 30602790]

(11). (a)Atzori C; Bruno A; Chichino G; Bombardelli E; Scaglia M; Ghione M Activity of Bilobalide, a Sesquiterpene from *Ginkgo biloba,* on *Pneumocystis carinii*. Antimicrob. Agents Chemother. 1993, 37, 7, 1492; [PubMed: 8363381] (b)Bombardelli E; Ghione M Pharmaceutical Uses of Bilobalide and Derivatives Thereof and Pharmaceutical Compositions Adapted for Such Use. U.S. Pat. Appl. US005264216A, 1993;(c)Bombardelli E; Ghione M Bilobalide Derivatives, Their Applications and Formulations Containing Them. US005202313A, 1993;(d)Bombardelli E; Ghione M Use of bilobalide and derivatives thereof for treating an infection in an individual and pharmaceutical compositions adapted for such use. EP0556051B1, 1997.

(12). (a)Pan L; Ren L; Chen F; Feng Y; Luo Y Anti-feedant Activity of *Ginkgo biloba* Secondary Metabolites against *Hyphantria cunea* Larvae: Mechanisms and Applications. PLoS ONE 2016, 11, 1;(b)Pszczolkowski MA; Durden K; Sellars S; Cowell B; Brown JJ Effects of *Ginkgo biloba* Constituents on Fruit-Infesting Behavior of Coding Moth (*Cydia pomonella*) in Apples. J. Agric. Food Chem 2011, 59, 10879–10886. [PubMed: 21905729] (c)Ahn YJ; Kwon M; Park HM; Han CK Potent Insecdticidal Activity of *Ginkgo biloba* Derived Trilactone Terpenes. ACS Symposium Series 1997, Ch. 7, 90;(d)Ozoe Y γ-aminobutyrate- and glutamate-gated chloride channels as targets of insecticides. Advances in Insect Physiology, 2013, 44, 211.

(13). Major RT The Ginkgo, the most ancient living tree, Science 1967, 157, 1270. [PubMed: 5341600]

(14). Koch E Inhibition of platelet activating factor (PAF)-induced aggregation of human thrombocytes by ginkgolides: considerations on possible bleeding complications after oral intake of *Ginkgo biloba* extracts. Phytomedicine 2005, 12, 10. [PubMed: 15693702]

(15). Lee D; Su H; O'Dowed DK GABA receptors Containing Rdl Subunits Mediate Fast Inhibitory Synaptic Transmission in *Drosophola* Neurons. J. Neuroscience 2003, 23, 4625.

(16). (a)Constant RHF; Steichen JC; Rocheleau TA; Aronstein K; Roush RT A single-amino acid substitution in a γ-aminobutyric acid subtype A receptor locus is associated with cyclodiene insecticide resistance in *Drosophila* populations. PNAS, 1993, 90, 1957; [PubMed: 8095336] (b)Thompson AJ; McGonigle I; Duke R; Johnston GAR; Lummis SCR A single amino acid determines the toxicity of *Ginkgo biloba* extracts. FASEB J. 2012, 26, 1884. [PubMed: 22253475]

(17). (a)Huang SH, Duke RK, Chebib M, Sasaki K, Wada K, and Johnston GA Bilobalide, a sesquiterpene trilactone from Ginkgo biloba, is an antagonist at recombinant, $\alpha_1\beta_2\gamma_{2L}$ $GABA_A$ receptors. Eur. J. Pharmacol 2003, 464, 1.; [PubMed: 12600688] (b)Ng CC; Duke RK; Hinton T; Johnston GAR $GABA_A$ receptor cysteinyl mutants and the ginkgo terpenoid lactones bilobalide and ginkgolides. Eur. J. Pharmacol 2016, 777, 136. [PubMed: 26953225]

(18). Kalueff AV Mapping convulsants' binding to the GABA-A receptor chloride ionophore: A proposed model for channel binding sites Neurochem. Int 2007, 57, 61.

(19). A note on nomenclature: residues in the transmembrane domain (TMD)-spanning α-helices (see Figure 1) are numbered from 0', a conserved charged residue near the cytoplasm. Negative numbered residues (e.g. −2') are farther from the extracellular domain and positive numbered residues are closer. See Ref. 16b.

(20). Ng CC; Duke RK; Hinton T; Johnston GAR Effects of Bilobalide, Ginkgolide B and Picrotoxinin on $GABA_A$ receptor Modulation by Structurally Diverse Positive Modulators. Eur. J. Pharmacol 2017, 806, 83. [PubMed: 28416372]

(21). (a)Jorgensen JL Aldrin and Dieldrin: A Review of Research on Their Production, Environmental Deposition and Fate, Bioaccumulation, Toxicology, and Epidemiology in the United States. Environ. Health Perspect 2001, 109, 113. [PubMed: 11250811] (b)Agency for Toxic Substances and Disease Registry (ATSDR). 2002 Toxicological profile for Aldrin/Dieldrin. Atlanta, GA: U.S. Department of Health and Human Services, Public Health Service.(c)Soto AR; Deichman WB; Major Metabolism and Acute Toxicity of Aldrin, Dieldrin, and Endrin. Environmental Research 1967, 1, 307. [PubMed: 4880048]

(22). (a)Lu HH; Martinez MD; Shenvi RA An eight-step- gram-scale synthesis of (−)-jiadifenolide. Nature Chem. 2015, 7, 604; [PubMed: 26100810] (b)Ohtawa M; Krambis MJ; Cerne R; Schkeryantz JM; Witkin JM Shenvi RA Synthesis of (−)-11-*O*-Debenzoyltashironin: Neurotrophic Sesquiterpenes Cause Hyperexcitation. J. Am. Chem. Soc 2017, 139, 9637. [PubMed: 28644021]

(23). Witkin et al. Pharmacological characterization of the neurotrophic sesquiterpenejiadifenolide reveals a non-convulsant signature and potential forprogression in neurodegenerative disease studies. Biochem. Pharmacol 2018, 155, 61. [PubMed: 29940173]

(24). Huffman BJ; Chen S; Schwarz JL; Plata RE; Chin E; Houk KN; Lairson LL; Ryan A Shenvi Electronic Complementarity Permits Hindered Butenolide Heterodimerization and Discovery of Novel cGAS/STING Pathway Antagonists, Nature Chem. 2020, 12, 310.

(25). Böttcher T An Additive Definition of Molecular Complexity. J. Chem. Inf. Model 2016, 56, 462. [PubMed: 26857537]

(26). Herzon SB Emergent Properties of Natural Products. SynLett 2018, 29, 1823.

(27). Weir CJ; Ling ATY; Belelli D; Wildsmith JAW; Peters JA; Lambert JJ The interaction of anaesthetic steroids with recombinant glycine and $GABA_A$ receptors. Br. J. Anaesth 2004, 92, 704. [PubMed: 15033889]

(28). (a)Corey EJ; Guo S Total synthesis of a C15 ginkgolide, (±)-bilobalide. J. Am. Chem. Soc 1987, 109, 7534.(b)Corey EJ; Su W Enantioselective Total Synthesis of Bilobalide, A C15 Ginkgolide. Tetrahedron Lett. 1988, 29, 3423.

(29). Crimmins MT; Jung DK; Gray JL Synthetic Studies on the Ginkgolides: Total Synthesis of (±)-Bilobalide. J. Am. Chem. Soc 1993, 115, 3155.

(30). Normalization by dividing by atom count mitigates the influence of protecting groups which often encode large amounts of information that is irrelevant to building target complexity.

(31). Baker MA; Demoret RM; Ohtawa M; Shenvi RA Concise asymmetric synthesis of (−)-bilobalide. Nature 2019, 575, 643. [PubMed: 31618759]

(32). Schuster DI; Lem G; Kaprinidis NA New Insights into an old Mechanism: [2+2] Photocycloadditions of Enones to Alkenes. Chem. Rev 1993, 93, 3.

(33). (a)Iwasaki K; Wan KK; Oppedisano A; Crossley SWM; Shenvi RA Simple, Chemoselective Hydrogenation with Thermodynamic Stereocontrol. J. Am. Chem. Soc 2014, 136, 1303; (b)Crossley SWM; Barabé F; Shenvi RA Simple, Chemoselective, Catalytic Olefin Isomerization, J. Am. Chem. Soc 2014, 136, 16788. [PubMed: 25398144]

(34). Crossley SWM; Martinez RM; Obradors C; Shenvi RA Mn, Fe, and Co-Catalyzed Radical Hydrofunctionalizations of Olefins, Chem. Rev 2016, 116, 8912. [PubMed: 27461578]

(35). Evans DA; Tedrow JS; Shaw JT; Downey CW Diastereoselective Magnesium Halide-Catalyzed *anti*-Aldol Reactions of Chiral *N*-Acyloxazolidinones. J. Am. Chem. Soc 2002, 124, 392. [PubMed: 11792206]

(36). Nicolaou KC; Ellery SP; Chen JS Samarium Diiodide-Mediated Reactions in Total Synthesis. Angew. Chem. Int. Ed 2009, 48, 39, 7140.

(37). Thankachan AP; Asha S; Singhu KS; Anilkumar G An overview of Zn-catalyzed enantioselective aldol type C-C bond formation. RSC Adv. 2015, 5, 62179.

(38). Kern N; Plesniak MP; McDouall JJW; Procter DJ Enantioselective cyclizations and cyclization cascades of samarium ketyl radicals. Nature Chem. 2017, 9, 1198. [PubMed: 29168498]

(39). Ribeiro CMR; Cordeiro de Farias FM Chiral Ligands in the Asymmetric Reformatsky Reaction. Mini-Reviews in Organic Chemistry. 2006, 3, 1.

(40). Ojida A; Yamano T; Taya N; Tasaka A Highly Enantioselective Reformatsky Reaction of Ketones: Chelation-Assisted Enantioface Discrimination. Org. Lett 2002, 4, 18, 3051. [PubMed: 12201714]

(41). Kloetzing RJ; Thaler T; Knochel P An Improved Asymmetric Reformatsky Reaction Mediated by (−)-*N,N*-Dimethylaminoisoborneol. Org. Lett 2006, 8, 1125. [PubMed: 16524284]

(42). Wolf C; Moskowitz M Bisoxazolidine-Catalyzed Enantioselective Reformatsky Reaction. J. Org. Chem 2011, 76, 6372. [PubMed: 21623640]

(43). Fernández-Ibáñez MA; Maciá B; Minnaard AJ; Feringa BL Catalytic Enantioselective Reformatsky Reaction with Aldehydes. Angew. Chem. Int. Ed 2008, 47, 1317.

(44). Lin N; Chen M-M; Luo R-S; Deng T-Q; Lu G Indolinylmethanol catalyzed enantioselective Reformatsky reaction with ketones. Tetrahedron: Asymm. 2010, 21, 2816.

(45). Cozzi PG; Mignogna A; Zoli L Catalytic enantioselective Reformatsky reactions. Pure Appl. Chem 2008, 80, 891.

(46). Kanai K; Wakabayashi H; Honda T Rhodium-Catalyzed Reformatsky-Type Reaction. Org. Lett 2000, 2, 2549. [PubMed: 10956544]

(47). Li Y; He B Asymmetric Reformatsky Reaction of Aldehydes Catalyzed by Novel *β*-amino Alcohols and Zinc Complexes. Synth. Commun 2014, 44, 13, 1938.

(48). Fornalczyk M; Singh K; Stuart AM Enantioselective Reformatsky reaction of ethyl iododifluoroacetate with ketones. Org. Biomol. Chem 2012, 10, 3332. [PubMed: 22421710]

(49). Fernández-Ibáñez MA; Maciá B; Alonso DA; Pastor IM Recent Advances in the Catalytic Enantioselective Reformatsky Reaction. Eur. J. Chem 2013, 7028.

(50). Choppin S; Ferreiro-Medeiros L; Barbarotto M; Colobert F Recent advances in the diastereoselective Reformatsky-type reaction. Chem. Soc. Rev 2013, 42, 937. [PubMed: 23212078]

(51). Li F; Castle SL Synthesis of the Acutumine Spiro-cycle via a Radical–Polar Crossover Reaction. Org. Lett 2007, 9, 4033. [PubMed: 17760457]

(52). Va P; Campbell EL; Robertson WM; Boger DL Total Synthesis and Evaluation of a Key Series of C5-Substituted Vinblastine Derivatives. J. Am. Chem. Soc 2010, 132, 8489. [PubMed: 20518465]

(53). Schröder M Osmium Tetraoxide Cis Hydroxylation of Unsaturated Substrates. Chem. Rev 1980, 80, 187.

(54). (a)Abelman MM; Oh T; Overman LE Intramolecular Alkene Arylations for Rapid Assembly of Polycyclic Systems Containing Quaternary Centers. A New Synthesis of Spirooxindoles and Other Fused and Bridged Ring Systems. J. Org. Chem 1987, 52, 4130;(b)Ludlow BS; Danielson J; Somfai PComino Carbopalladation-Carbonylation: Investigation Substrate Scope. Adv. Synth. Catal 2012, 354, 206;(c)Liu P; Seo JH; Weinreb SM Total Synthesis of the Polycyclic Fungal Metabolite (±)-Communesn F. Angew. Chem. Int. Ed 2010, 49, 2000.

(55). (a)Zombeck A; Hamilton DE; Drago RS Novel Catalytic Oxidations of Terminal Olefins by Cobalt(II)-Schiff Base Complexes. J. Am. Chem. Soc 1982, 104, 6782.(b)Mukaiyama T; Isayama S; Inoki S; Kato K; Yamada T; Takai T Oxidation-reduction hydration of olefins with molecular oxygen and 2-propanol catalyzed by bis(acetylacetonato)cobalt(II). Chem. Lett 1989, 18, 449.

(56). Green SA; Crossley SWM; Matos JLM; Vásquez-Céspedes S; Shevick S; Shenvi RA The High Chemofidelity of Metal-Catalyzed Hydrogen Atom Transfer. Acc. Chem. Res 2018, 51, 2628. [PubMed: 30406655]

(57). Yaremenko IA; Vil VA; Demchuk DV; Terent'ev AO. Rearrangements of organic peroxides and related processes. Beilstein J. Org. Chem 2016, 12, 1647. [PubMed: 27559418]

(58). Nishinaga A; Yamada T; Fujisawa H; Ishizaki K; Ihara H; Matsuura T Catalysis of Cobalt-Schiff Base Complexes In Oxygenation of Alkenes: On the Mechanism of Ketonization. J. Mol. Catal 1988, 48, 249.

(59). Only recently has absolute stereocontrol emerged. See: (a) Discolo CA; Touney EE; Pronin SV Catalytic Asymmetric Radical–Polar Crossover Hydroalkoxylation. J. Am. Chem. Soc 2019, 44, 17527;(b)Ebisawa K; Izumi K; Ooka Y; Kato H; Kanazawa S; Komatsu S; Nishi E; Shigehisa H Catalyst- and Silane-Controlled Enantioselective Hydrofunctionalization of Alkenes by Cobalt-Catalyzed Hydrogen Atom Transfer and Radical-Polar Crossover. J. Am. Chem. Soc 2020, 142, 13481. [PubMed: 32648757]

(60). Zuckerman DS; Woerpel KA Diastereoselective peroxidation of derivatives of Baylis-Hillman adducts. Tetrahedron 2019, 75, 4118. [PubMed: 32831414]

(61). Obradors C; Martinez RM; Shenvi RA Ph(*i*-PrO)SiH_2: An Exceptional Reductant for Metal-Catalyzed Hydrogen Atom Transfers. J. Am. Chem. Soc 2016, 138, 4962. [PubMed: 26984323]

(62). Parsons AF; Bar G Stereoselective radical reactions. Chem. Soc. Rev 2003, 32, 251; [PubMed: 14518178] (b)Hanessian S; Yang H; Schaum R Hydrogen-Bonding as a Stereocontrolling Element in Free-Radical C-Allylation Reactions: Vicinal, Proximal, and Remote Asymmetric Induction in the Amino Acid Series. J. Am. Chem. Soc 1996, 118, 2507;(c)Pedrosa R; Andrés C; Duque-Soladana JP; Mendiguchía P A Novel Case of Diastereoselection in 5-exo Radical Cyclization Promoted by Hydrogen Bonding Eur. J. Org. Chem 2000, 3727;(d)Guindon Y; Guérin B; Landry SR, Intramolecular Aminyl and Iminyl Radical Additions to α,β-Unsaturated Esters. Diastereoselective Tandem Cyclofunctionalization and Hydrogen Transfer Reactions. Org. Lett 2001, 3, 2293. [PubMed: 11463299]

(63). Heathcock CH; Kath JC; Ruggeri RB. *Daphniphyllum* Alkaloids. 16. Total Synthesis of (+)-Codaphniphylline. J. Org. Chem 1995, 60, 1120.

(64). Xue F; Gu W; Silverman RB Concise Route to the Chiral Pyrrolidine Core of Selective Inhibitors of Neuronal Nitric Oxide. Org. Lett 2009, 11, 5194. [PubMed: 19860389]

(65). González DF; Brand JP; Waser J Ethynyl-1,2-benziodoxol-3(1*H*)-one (EBX): An Exceptional Reagent for the Ethynylation of Keto, Cyano, and Nitro Esters. Chem. Eur. J 2010,16, 9457. [PubMed: 20645361]

(66). Yudasaka M; Shimbo D; Maruyama T; Tada N; Itoh A Synthesis, Characterization, and Reactivity of an Ethynyl Benziodoxolone (EBX)–Acetonitrile Complex. Org. Lett 2019, 21, 1098. [PubMed: 30707031]

(67). 3,5-dinitrobenzoate **33** was isolated and characterized, but it decomposed via facile benzoate hydrolysis during multiple crystallization attempts. The bis-(ethyl ester) corresponding to **33** was much more stable and easily crystallized (see Supporting Information).

(68). (a)Bhagwat SS, Hamann PR, Still WC Synthesis of Thromboxane A2. J. Am. Chem. Soc. 1985, 107, 6372;(b)for a beautiful structural modification to impart acid stability, see: Jing C; Mallah S; Kriemen E; Bennett SH; Fasano V; Lennox AJJ; Hers I; Aggarwal VK Synthesis, Stability, and Biological Studies of Fluorinated Analogues of Thromboxane A2 ACS Cent. Sci 2020, 6, 995. [PubMed: 32607446]

(69). Bull JA; Croft RA; Davis OA; Doran R; Morgan KF Oxetanes: Recent Advances in Synthesis, Reactivity, and Medicinal Chemistry. Chem. Rev 2016, 116, 12150. [PubMed: 27631342]

(70). Wu E, Kong F, Synthesis and Conformational Analysis of Substituted 2,6-dioxabicyclo[3.3.1]heptanes: 1,3-anhydro-2,4-di-*O*-benzyl- and -2,4-di-*O*-(*p*-bromobenzyl)-β-L-rhamnopyranose, Carbohydrate Res. 1987, 161, 235.

(71). Shimada N; Hasegawa S; Harada T; Tomisawa T; Fujii A; Takita T Oxetanocin, a Novel Nucleoside from Bacteria J. Antibiotics 1986, 39, 1623.

(72). Han Q; Zhang J; Lu Y; Wu Y; Zheng Q; Sun H A Novel Cytotoxic Oxetane *ent*-Kauranoid from *Isodon japonicus*. Planta Med. 2004, 70, 581. [PubMed: 15318402]

(73). Emsermann J; Opatz T; Photochemical Approaches to the Bilobalide Core. Eur. J. Org. Chem 2017, 3362.

(74). Maier G; Pfriem S; Schäfer U; Matusch R Tetra-*tert*-butyltetrahedrane. Angew. Chem. Int. Ed. Engl 1978, 17, 520.

(75). Evans DA; Kaldor SW; Jones T K; Clardy, J.; Stout, T. J. Total synthesis of the macrolide antibiotic cytovaricin J. Am. Chem. Soc 1990, 112, 7001.

(76). Vedejs E; Chen X Parallel Kinetic Resolution. J. Am. Chem. Soc 1997, 119, 2584.

(77). (a)Coric I, Muller S, List B Kinetic Resolution of Homoaldols via Catalytic Asymmetric Transacetalization. J. Am. Chem. Soc 2010, 132, 17370; [PubMed: 21087021] (b)Sun Z; Winschel GA; Borokiva A; Nagorny P Chiral phosphoric acid-catalyzed enantioselective and diastereoselective spiroketalizations. J. Am. Chem. Soc 2012, 134, 8074. [PubMed: 22545651]

(78). We validated dr by NMR to avoid LC errors based on differential UV-activity, ionization of diastereomers, or impurity co-elution.

(79). (a)Shu C; Liu MQ; Sun YZ; Ye LW Efficient Synthesis of γ-Lactones via Gold-Catalyzed Tandem Cycloisomerization/Oxidation. Org. Lett 2012, 14, 4958; [PubMed: 22931371] (b)Zeng M; Herzon SB Synthesis of 1,3-Amino Alcohols, 1,3-Diols, Amines, and Carboxylic Acids from Terminal Alkynes. J. Org. Chem 2015, 80, 8604; [PubMed: 26203776] (c)Asao N; Ohishi T; Sato K; Yamamoto Y Lewis acid catalyzed stereoselective hydrosilylation of ketones under the control of σ-π chelation. Tetrahedron, 2002, 58, 8195.

(80). Julia M; Saint-Jalmes VP; Verpeaux J-N Oxidation of Carbanions with Lithium *Tert*-Butyl Peroxide. Synlett 1993, 233.

(81). Ohtawa O; Ogihara S; Sugiyama K; Shiomi K; Harigaya Y; Nagamitsu T; Ōmura S Enantioselective total synthesis of atpenin A5. J. Antibiot 2009, 62, 289.

(82). Brown HC; Bhat NG; Srebnik M A Simple, General Synthesis of 1-Alkynyldiisopropoxyboranes. Tet. Lett 1988, 29, 2631.

(83). This reaction was conceived and executed in October 2017 by Dr. Masaki Ohtawa, presented in November 2017 at ISONIS-11, posted to ChemRxiv (May 30, 2019) and published in Ref. 31 (October 16, 2019). A variation on this same reaction was published recently (March 27, 2020): Li C; Zhao P; Li R; Zhang B; Zhao W. Oxidation of Alkynyl Boronates to Carboxylic Acids, Esters, and Amides. Angew. Chem. Int. Ed 2020, 59, 10913. A revised manuscript now cites our work.

(84). Nakanishi K; Habaguchi K; Nakadaira Y; Woods MC; Maruyama M; Major RT; Alauddin M; Patel AR; Weinges K; Baehr W Structure of bilobalide, a rare *tert*-butyl containing sesquiterpenoid related to the C20-ginkgolides. J. Am. Chem. Soc 1971, 93, 3544.

(85). (a)Lichtblau D; Berger JM; Nakanishi K Efficient Extraction of Ginkgloides and Bilobalde from *Ginkgo biloba* Leaves J. Nat. Prod 2002, 65, 1501; [PubMed: 12398553] (b)van Beek TA Chemical analysis of *Ginkgo biloba* leaves and extracts J. Chromatogr. A 2002, 967, 21; [PubMed: 12219929] (c)Jaracz S; Malik S; Nakanishi K Isolation of ginkgolides A, B, C, J and bilobalide from G. biloba extracts. Phytochemistry 2004, 65, 2897; [PubMed: 15501258] (d)Choi YH; Kim J; Yoo KP Eupercritical-Fluid Extraction of Bilobalide and Ginkgolides from *Ginkgo biloba* Leaves by Use of a Mixture of Carbon Dioxide, Methanol, and Water Chromatographia 2002, 56, 753;(e)Lang Q; Wai CM, Pressurized water extraction (PWE) of terpene trilactones from *Ginkgo biloba* leaves Green Chemistry 2003, 5, 415.

(86). Van Beek TA Comments on 'An Extraction Method for Determination of Ginkgolides ad Bilobalide in Ginkgo Leaf Extracts' Anal. Chem 2000, 72, 3396. [PubMed: 10939420]

(87). Fourtillan JB; Brisson AM; Girault J; Ingrand I; Decourt JP; Drieu K; Jouenne P; Biber A Pharmacokinetic properties of Bilobalide and Ginkgolides A and B in healthy subjects after intravenous and oral administration of Ginkgo biloba extract (EGb 761). Thérapie 1995, 50, 137. [PubMed: 7631288]

(88). Wang J; Ouyang J; Liu Y; Jia X; You S; He S; Di X Development of a sensitive LC–MS/MS method for the determination of bilobalide in rat plasma with special consideration of *ex vivo* bilobalide stability: Application to a preclinical pharmacokinetic study. J. Pharm. Biomed. Anal 2014, 95, 238. [PubMed: 24704454]

(89). Weinges K; Hepp M; Huber-Patz U; Rodewald H; Irngartinger H Chemie Der Ginkgolide, I. 10-Acetyl-1-Methoxycarbonyl-2,3,14,15,16-Pentanorginkgolid A, Ein Zwischenprodukt Zur Herstellung von Bilobalid. Liebigs Ann. der Chemie 1986, 6, 1057.

(90). Lanthier GF; Graham WAG π-Bonding in the Boron–Oxygen Bond. Chem. Comm 1968, 715.

(91). Juaristi E; Cuevas G Recent Studies of the Anomeric Effect. Tetrahderon 1992, 48, 5019.

(92). Luger P; Kothe, Paulsen, H. Krisallstructur von 2,3,4-tri-*O*-acetyl-β-D-xylopyranosylchloride. Carbohydr. Res 1974, 37, 283.

(93). For example, acetylation of amides to imides lowers α-CH acidity: Bordwell FG; Fried HE Heterocyclic Aromatic Anions with 4n + 2 π-electrons. J. Org. Chem 1991, 56, 4218.

(94). Kochkodan V; Darwish NB; Hilal N The chemistry of boron in water, in: Kabay N; Bryjak M; Hilal N (Eds.), Boron Separation Processes, Elsevier, Amsterdam, 2015.

(95). Chuang KV; Xu C; Reisman SEA 15-step synthesis of (+)-ryanodol. Science 2016, 353, 912. [PubMed: 27563092]

(96). Related derivatives of **2** yielded similar pKa difference between inner/outer lactones (details in SI).

(97). Shenvi RA Neurite Outgrowth Enhancement by Jiadifenolide: Possible Targets. Nat. Prod. Rep. 2016, 33, 535. [PubMed: 26891462]

(98). Roberto M, Kirson D & Khom S The Role of the Central Amygdala in Alcohol Dependence. Cold Spring Harb Perspect. Med 2020 doi: 10.1101/cshperspect.a039339.

(99). Herman MA; Contet C; Justice NJ; Vale W; Roberto M Novel subunit-specific tonic GABA currents and differential effects of ethanol in the central amygdala of CRF receptor-1 reporter mice. J. Neurosci 2013, 33, 3284. [PubMed: 23426657]

(100). Pirker S; Schwarzer C; Wieselthaler A; Sieghart W; Sperk G GABA(A) receptors: immunocytochemical distribution of 13 subunits in the adult rat brain. Neuroscience 2000, 101, 815. [PubMed: 11113332]

(101). Gilpin NW; Herman MA; Roberto M The central amygdala as an integrative hub for anxiety and alcohol use disorders. Biol. Psychiatry 2015, 77, 859. [PubMed: 25433901]

(102). Roberto M; Cruz MT; Gilpin NW; Sabino V; Schweitzer P; Bajo M; Cottone P; Madamba SG; Stouffer DG; Zorrilla EP; Koob GF; Siggins GR Parsons LH Corticotropin releasing factor-induced amygdala gamma-aminobutyric Acid release plays a key role in alcohol dependence. Biol. Psychiatry 2010, 67, 831. [PubMed: 20060104]

(103). Lovering F; Bikker J; Humblet C Escape from Flatland: Increasing Saturation as an Approach to Improving Clinical Success. J. Med. Chem 2009, 52, 6752. [PubMed: 19827778]

(104). For use in complexity-generation and biological annotation by ‘cell-painting,’ see: Gerry CJ; Hua BK; Wawer MJ; Knowles JP; Nelson SD Jr.; Verho O; Dandapani S; Wagner BK; Clemons PA; Booker-Milburn KI; Boskovic ZV; Schreiber SL Real-Time Biological Annotation of Synthetic Compounds. J. Am. Chem. Soc 2016, 138, 8920. [PubMed: 27398798]

(105). Bertz SH The first general index of molecular complexity” J. Am. Chem. Soc 1981, 103, 3599.

(106). Code and updates can be found at: https://github.com/ccsb-scripps/bottchscore This code has also been integrated into a web service: a SMILES string from ChemDraw can be converted to its Cm value at: https://forlilab.org/services/bottcher/.

(107). Li J; Eastgate MD Current complexity: a tool for assessing the complexity of organic molecules, Org. Biomol. Chem 2015, 13, 7164. [PubMed: 25962620]

(108). Crossley SWM; Tong G; Lambrecht M; Burdge HE; Shenvi RA Synthesis of Picrotoxinin via Late-Stage Strong Bond Activations, J. Am. Chem. Soc 2020, 142, 1 1376.

(109). Huffman B; Shenvi RA Natural Products in the ‘Marketplace’: Interfacing Synthesis and Biology. J. Am. Chem. Soc 2019, 141, 3332. [PubMed: 30682249]

(110). Corey EJ; Wipke WT Computer-assisted design of complex organic synthesis, Science 1969, 166, 178. [PubMed: 17731475]

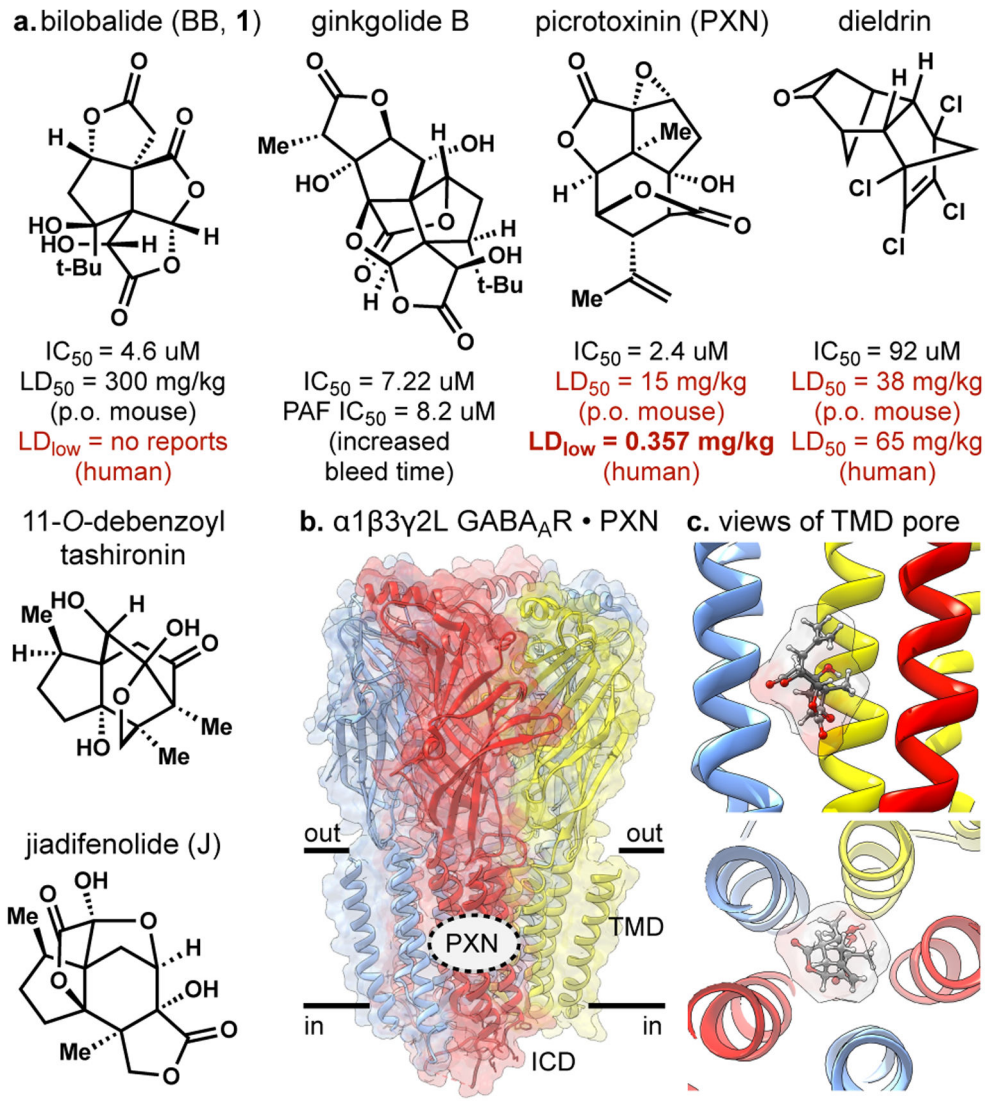

Figure 1.

a. Hyperexcitatory compounds that antagonize $GABA_A$ receptors; **b.** cryogenic electron microscopy structure of the human α1β3γ2L $GABA_A$ receptors; **c.** channel binding site of picrotoxinin, which exhibits allosteric coupling to the extracellular region (**b**/**c**, Ref. 10).

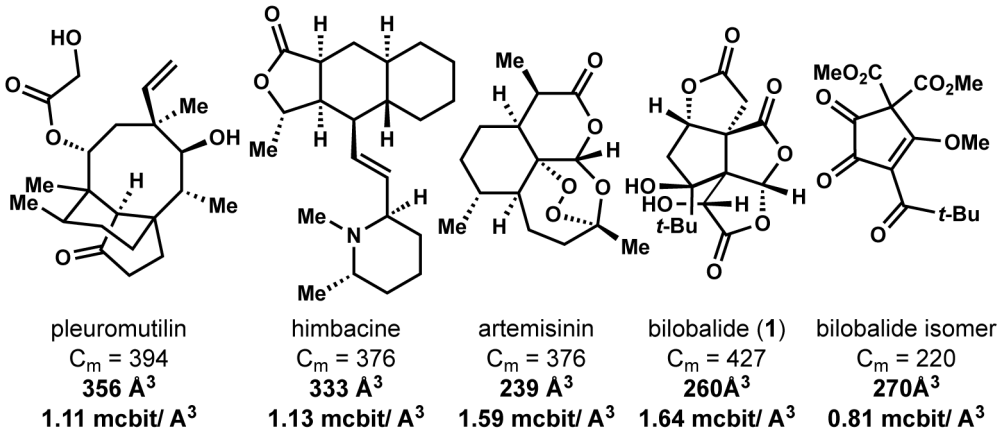

Figure 2.
Representative secondary metabolites, volumes and information densities.

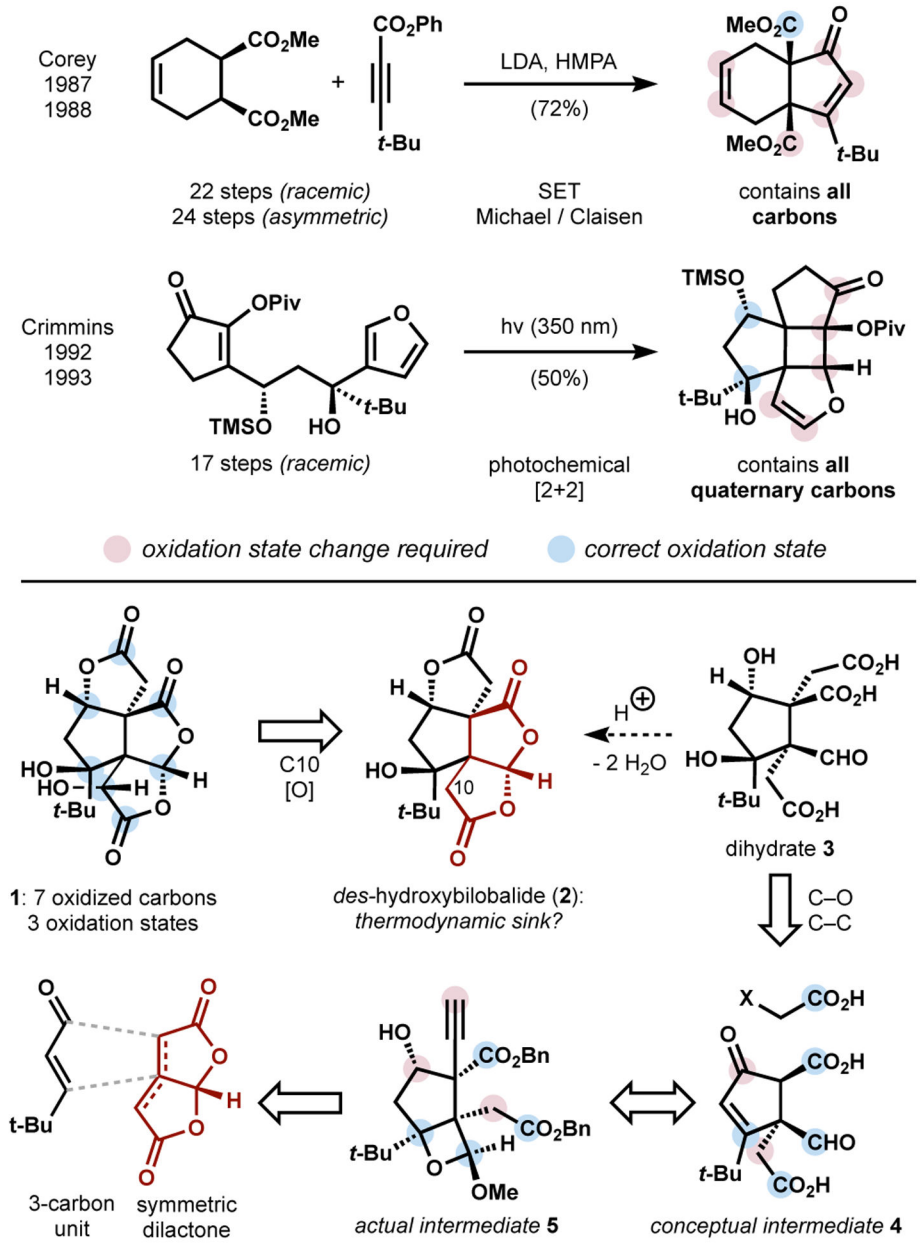

Figure 3.

Previous syntheses of **1** relied on early carbon framework synthesis, followed by oxidation state changes. The work here uses mostly preoxidized building blocks.

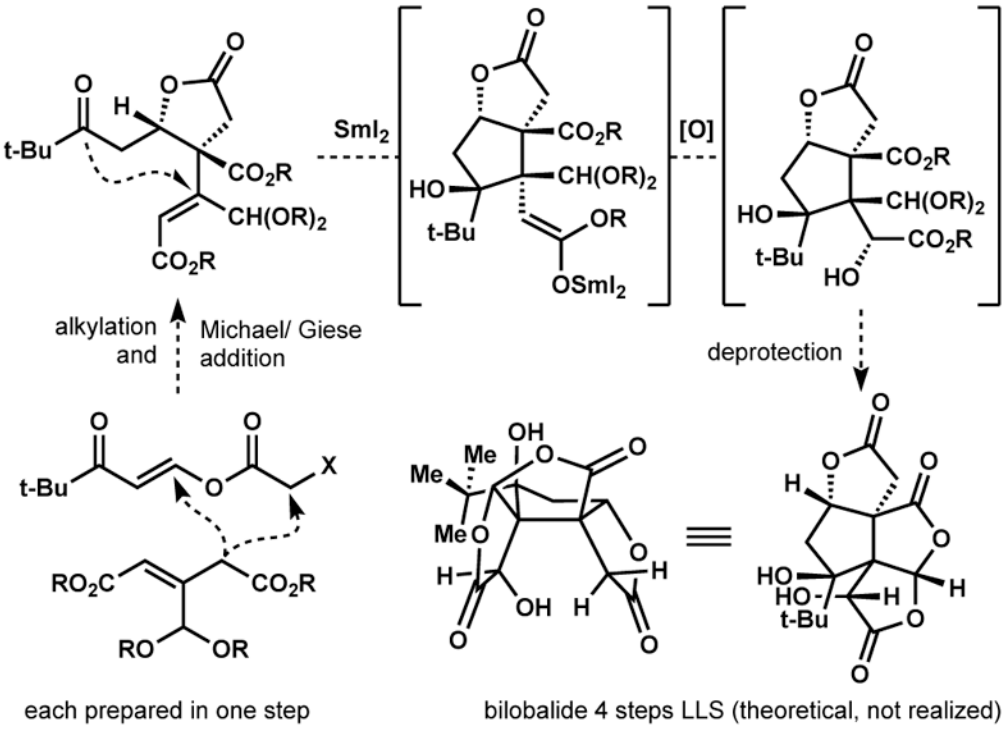

Figure 4.
An early approach using a pseudosymmetric building block and radical cyclization.

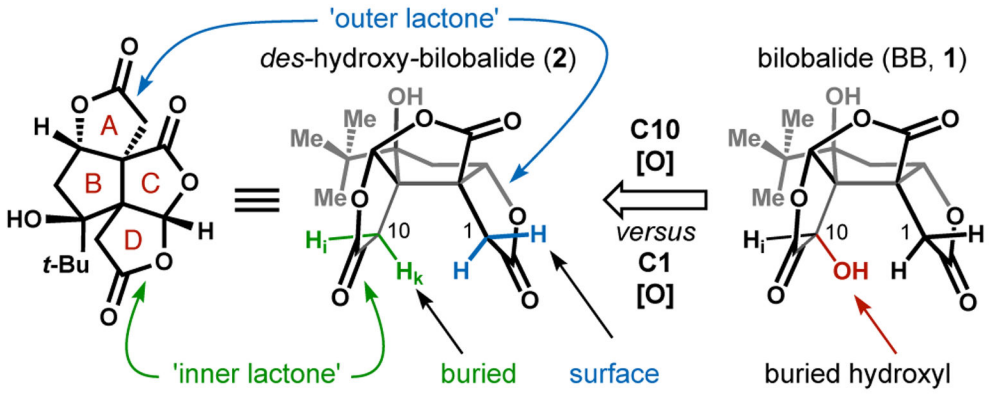

Figure 5.
Structural analysis of BB and identification of the topological problem with late stage oxidation.

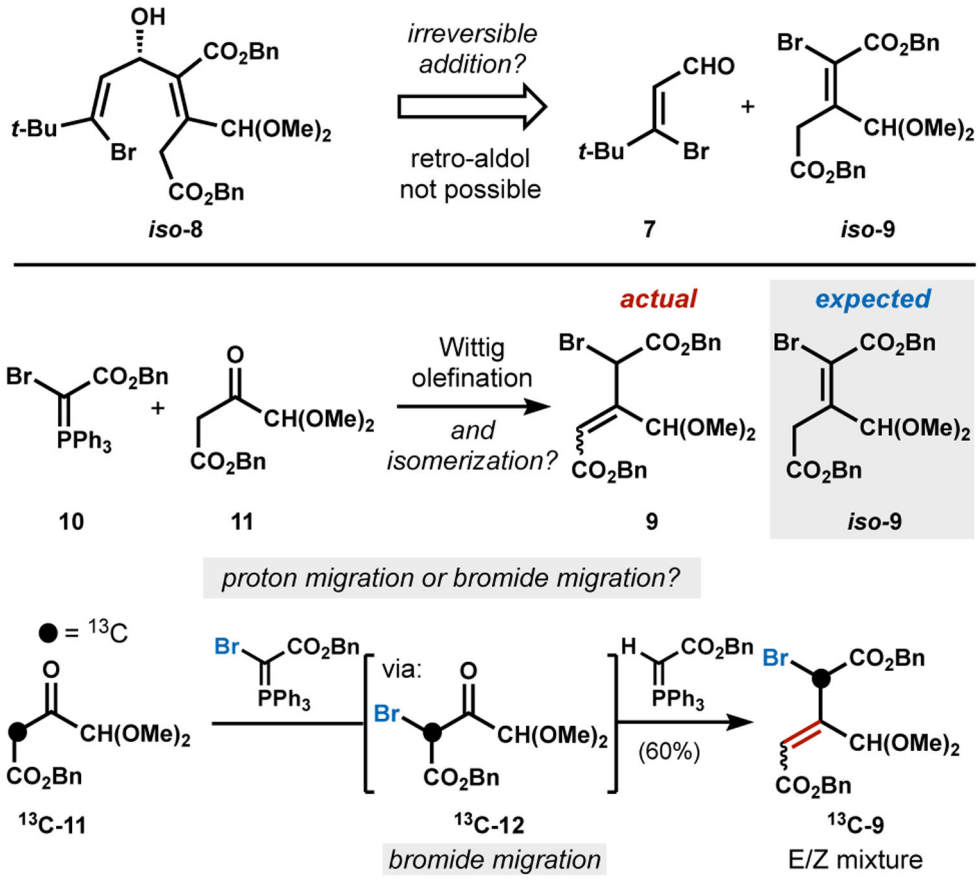

Figure 6.

^{13}C isotope labeling identifies bromide migration as operating in preference to proton migration.

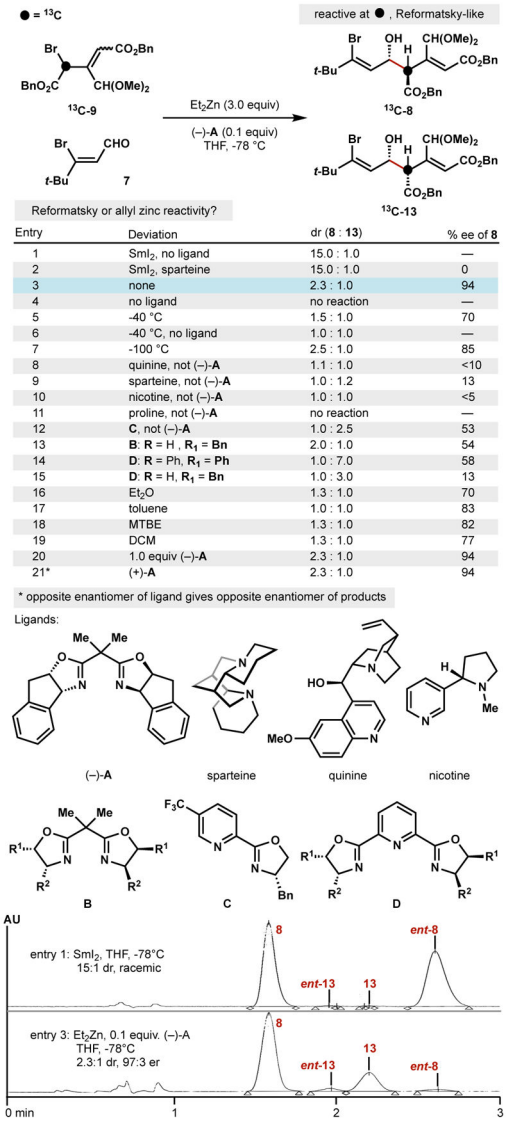

Figure 7.

Development of a catalytic asymmetric Reformatsky reaction. ^{13}C isotope labeling identifies *alpha*-attack operating in preference to *gamma*-attack.

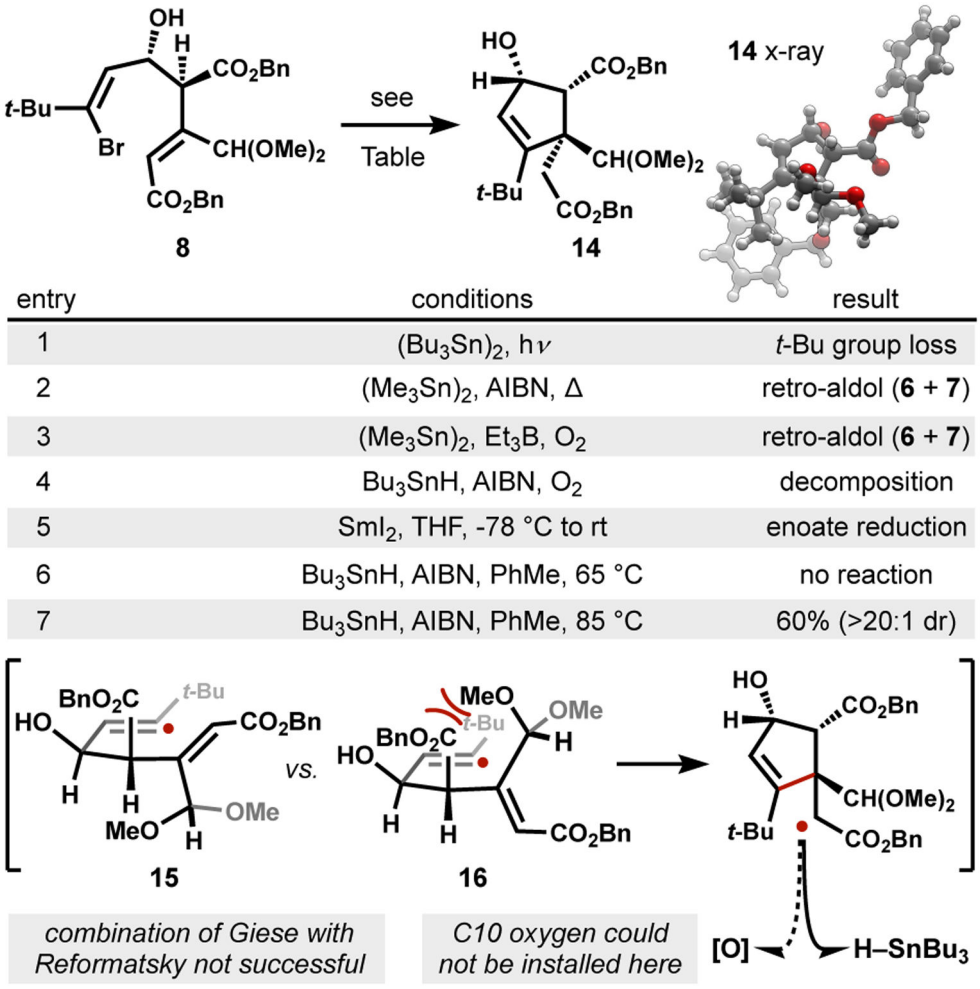

Figure 8.
Diastereoselective Giese addition.

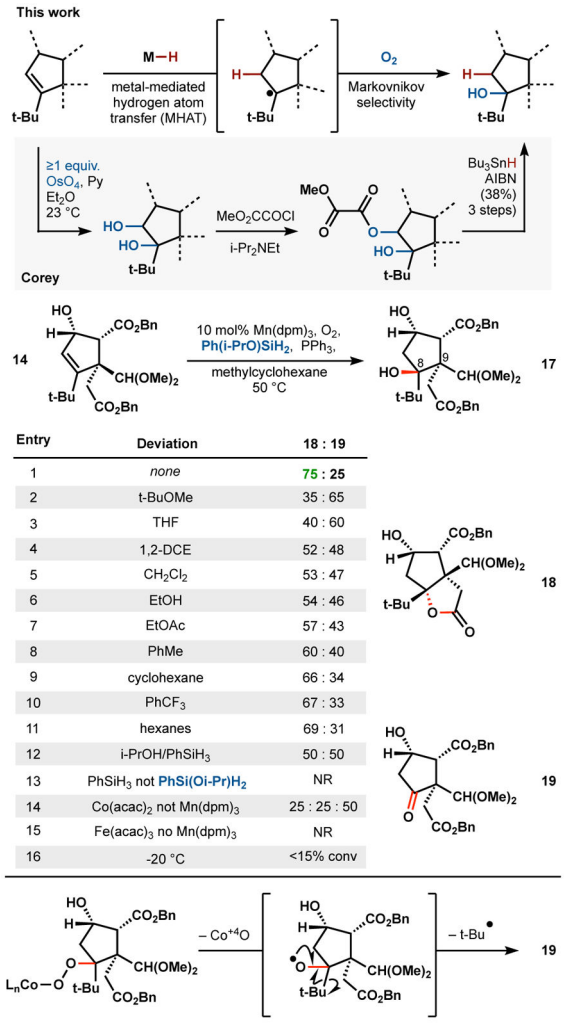

Entry	Deviation	18 : 19
1	*none*	**75 : 25**
2	t-BuOMe	35 : 65
3	THF	40 : 60
4	1,2-DCE	52 : 48
5	CH_2Cl_2	53 : 47
6	EtOH	54 : 46
7	EtOAc	57 : 43
8	PhMe	60 : 40
9	cyclohexane	66 : 34
10	$PhCF_3$	67 : 33
11	hexanes	69 : 31
12	i-PrOH/$PhSiH_3$	50 : 50
13	$PhSiH_3$ not $PhSi(Oi\text{-}Pr)H_2$	NR
14	$Co(acac)_2$ not $Mn(dpm)_3$	25 : 25 : 50
15	$Fe(acac)_3$ no $Mn(dpm)_3$	NR
16	-20 °C	<15% conv

Figure 9.

Effect of solvent, metal center and phosphine on Mukaiyama hydration probed using Ph(*i*-PrO)SiH_2.

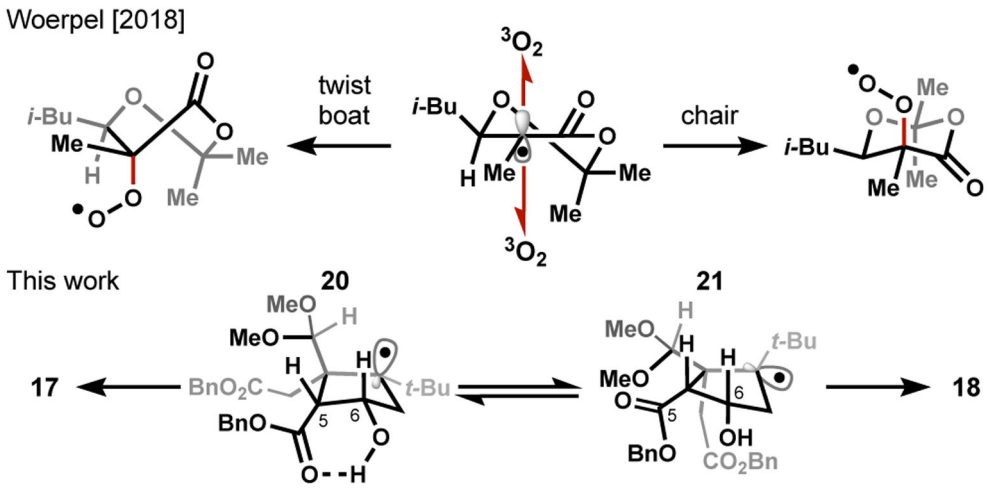

Figure 10.

Stereoselectivity via proposed chair versus twist-boat transition state conformations, compared with interconverting envelopes.

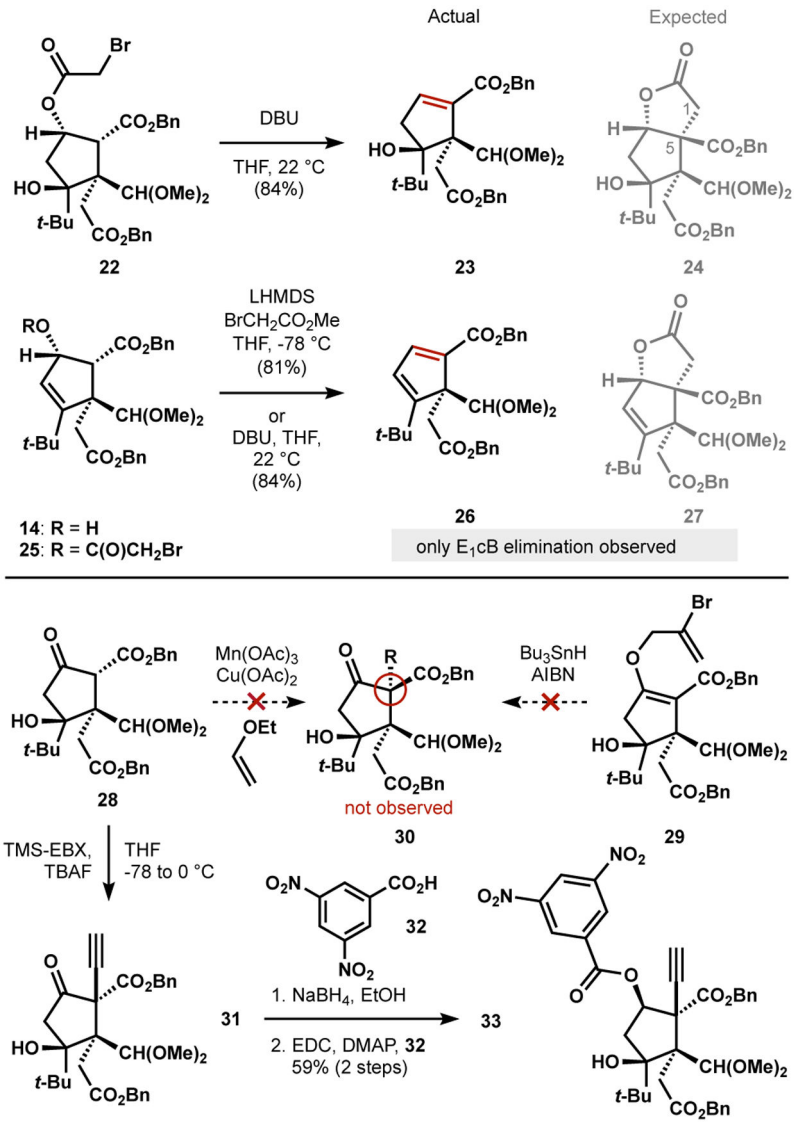

Figure 11.
Attempts to install final two-carbon unit at C5.

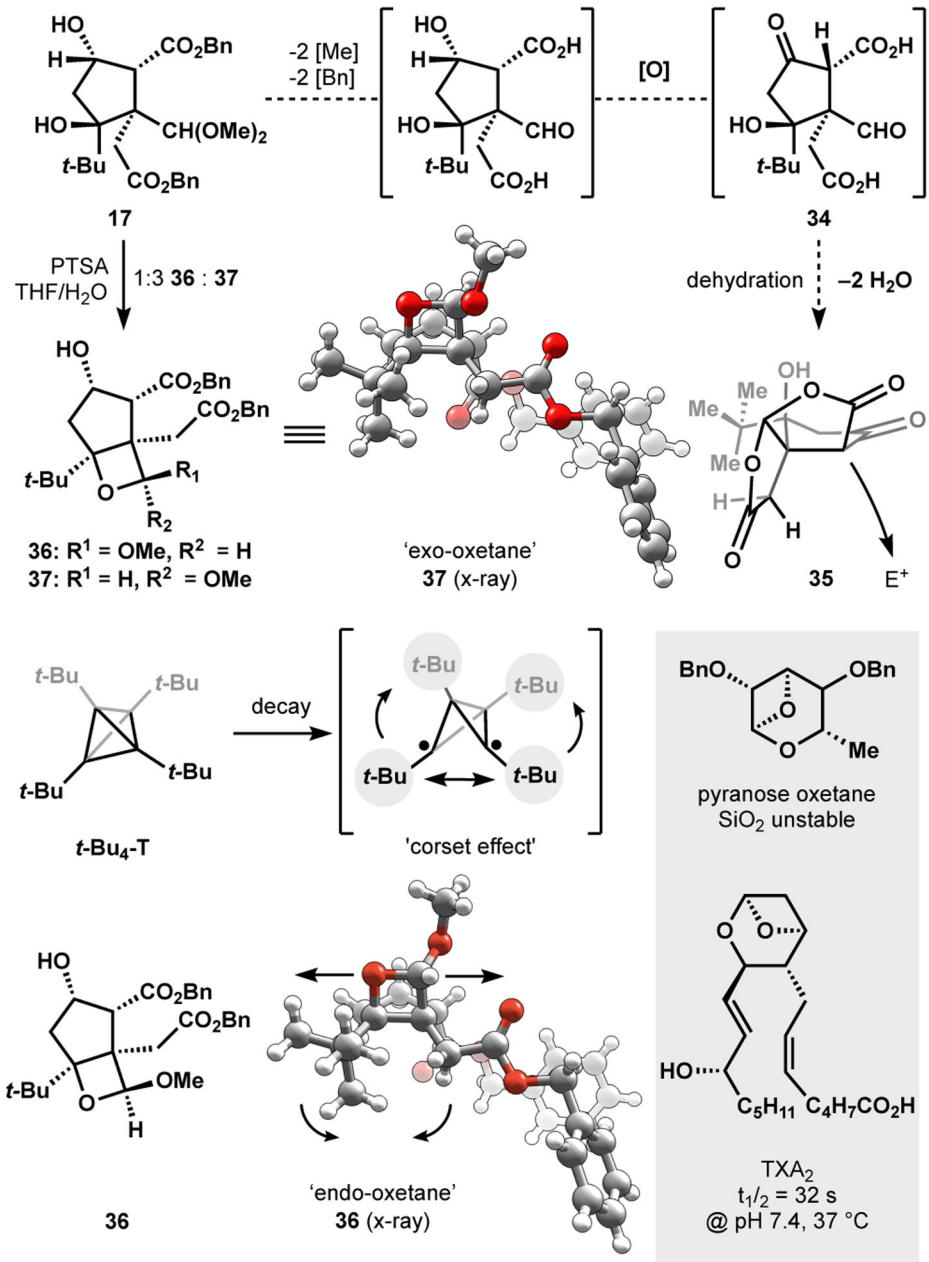

Figure 12.

Unexpected *trans*-acetalization to an acid-stable oxetane acetal driven by Maier's hypothetical 'corset' effect, where bulky groups destabilize the bond-lengthening decomposition.

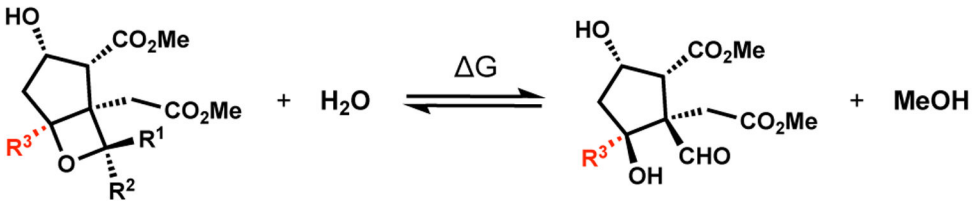

36_{calc}: R^1 = OMe, R^2 = H
37_{calc}: R^1 = H, R^2 = OMe

39a–d

	DMSO		THF		H_2O	
R^3	36_{calc}	37_{calc}	36_{calc}	37_{calc}	36_{calc}	37_{calc}
a: *t*-Bu	+2.2	+2.1	+2.0	+2.1	+5.6	+5.2
b: *i*-Pr	-0.2	-0.1	-0.5	-0.2	+1.1	+3.3
c: Me	-2.0	-2.4	-2.3	-2.4	+1.2	+1.0
d: H	-9.4	-9.1	-9.5	-9.0	-5.5	-6.1

Figure 13.
Calculated reaction free energies (kcal/mol) for the hydrolysis of oxetane acetals at the ωB97X-D/6-311++G(d,p), SMD//ωB97X-D/6-31+G(d,p) level of theory.

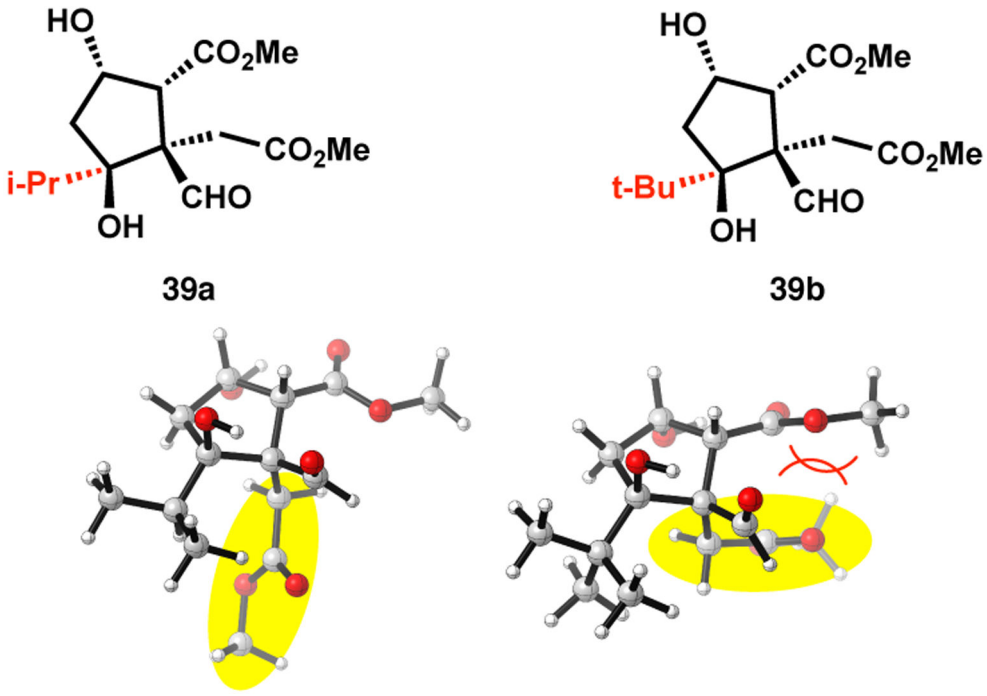

Figure 14.
Calculated structures of aldehydes **39a** and **39b** at the ωB97X-D/6-31+G(d,p) level of theory.

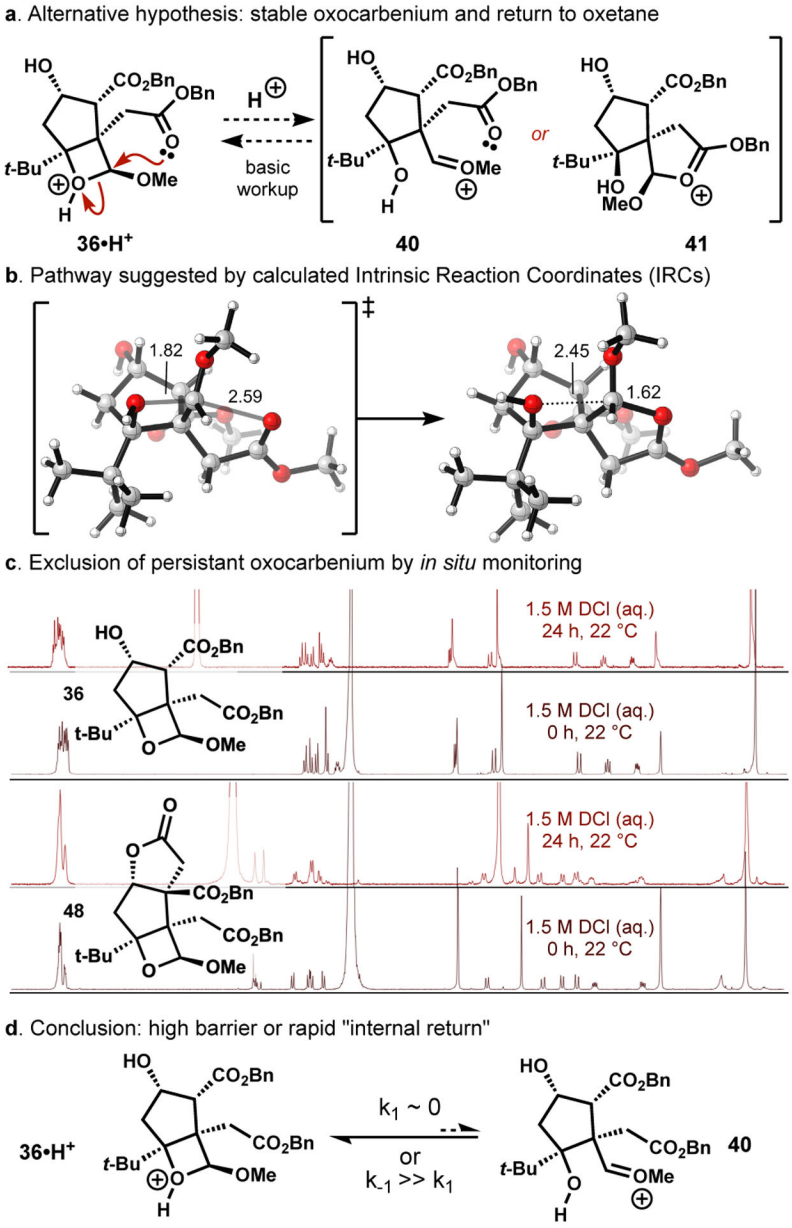

Figure 15.

The alternative hypothesis of an intermediate oxocarbenium that persists in acidic media, but reverts to oxetane in basic media, was excluded.

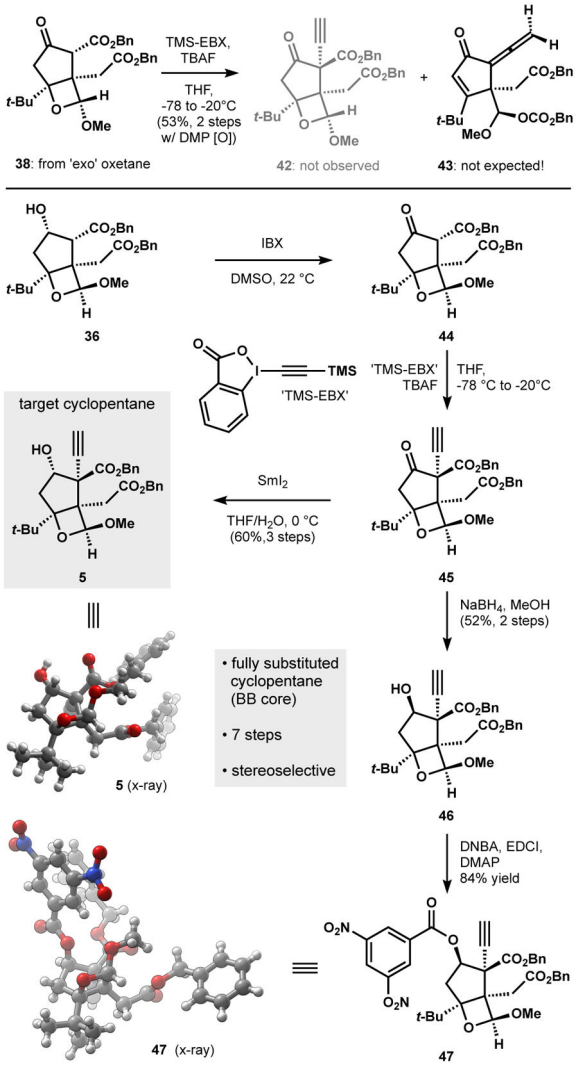

Figure 16.

endo-Oxetane **36** allows stereoselective alkynylation whereas *exo*-oxetane **37** rearranges. Hydride reductants deliver the wrong stereoisomer but SmI_2 accesses the fully substituted cyclopentane **48**, a total of 7 steps from commercial materials.

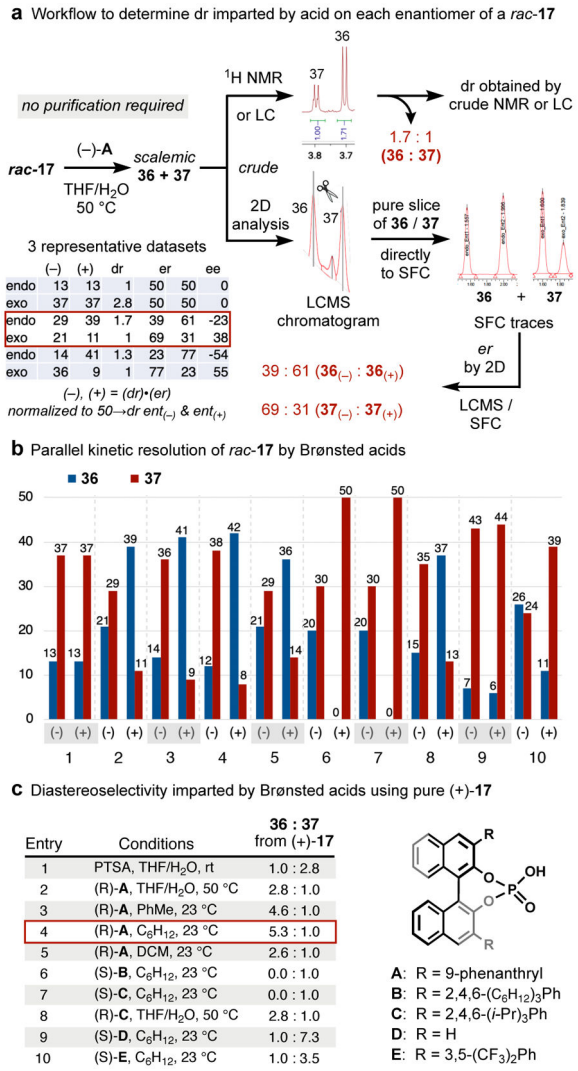

Figure 17.

Optimization of acetalization dr via parallel kinetic resolution (PKR): workflow and data analysis (SI22).

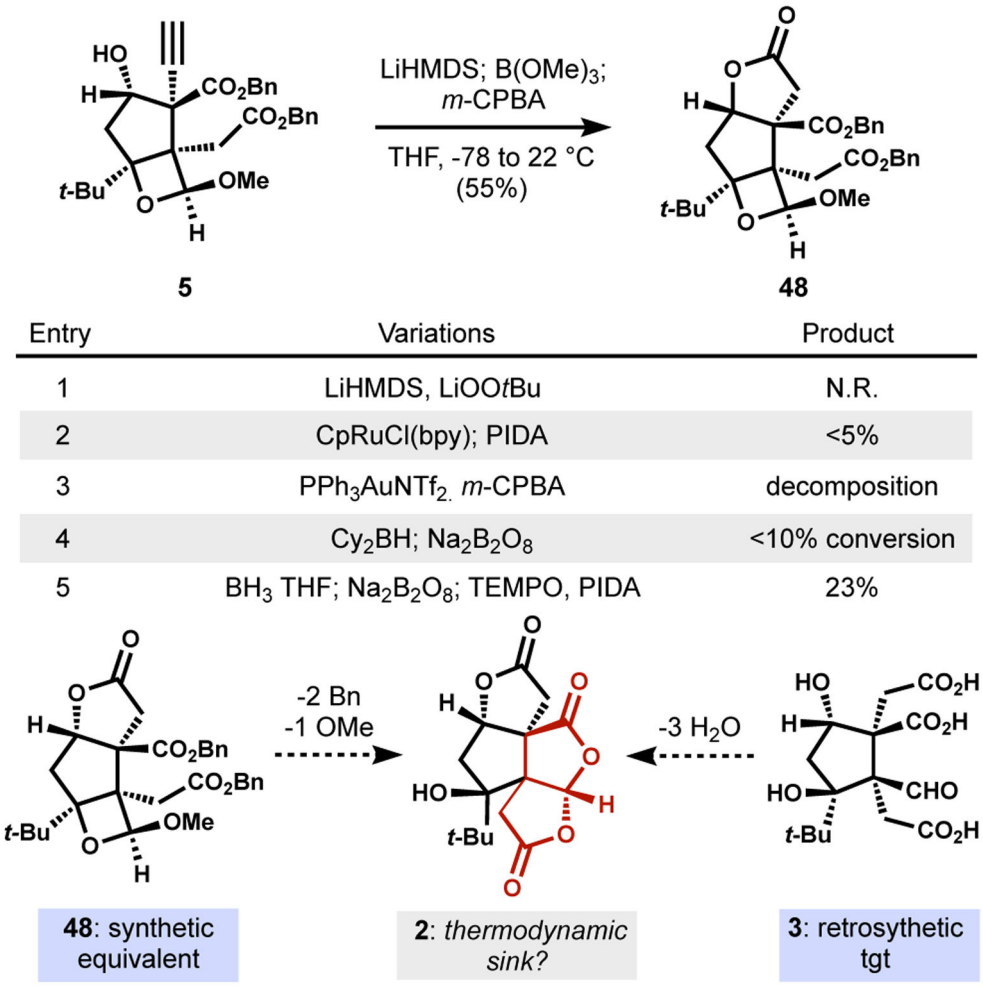

Entry	Variations	Product
1	LiHMDS, LiOO*t*Bu	N.R.
2	CpRuCl(bpy); PIDA	<5%
3	PPh_3AuNTf_2, *m*-CPBA	decomposition
4	Cy_2BH; $Na_2B_2O_8$	<10% conversion
5	BH_3 THF; $Na_2B_2O_8$; TEMPO, PIDA	23%

Figure 18.

Alkyne to lactone conversion via spborylation/oxidation versus other tactics. The resulting synthetic equivalent to **2** did not obviously resemble the retrosynthetic target.

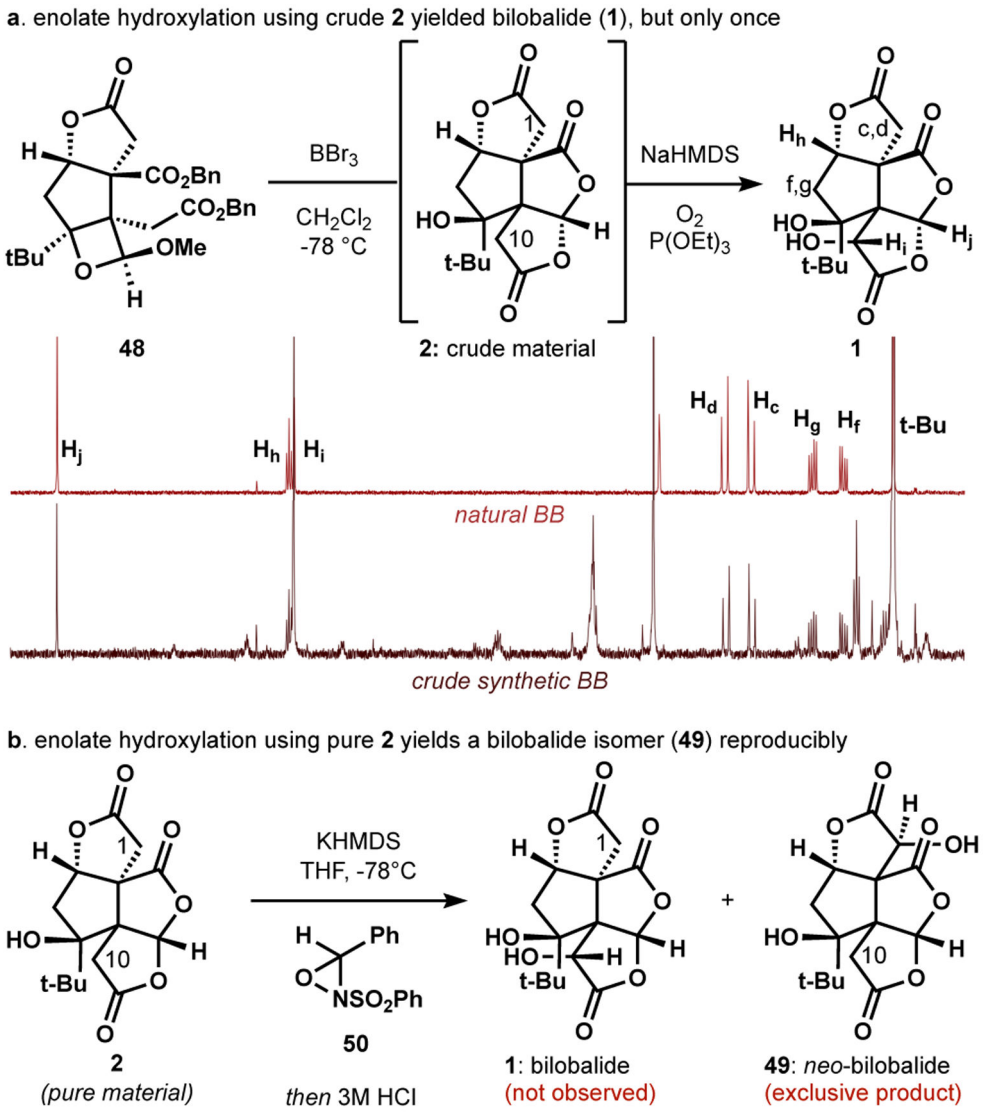

Figure 19.

a. BBr_3 deprotection/ O_2 oxidation of crude material delivered bilobalide (**1**) on the first attempt and **b.** never again.

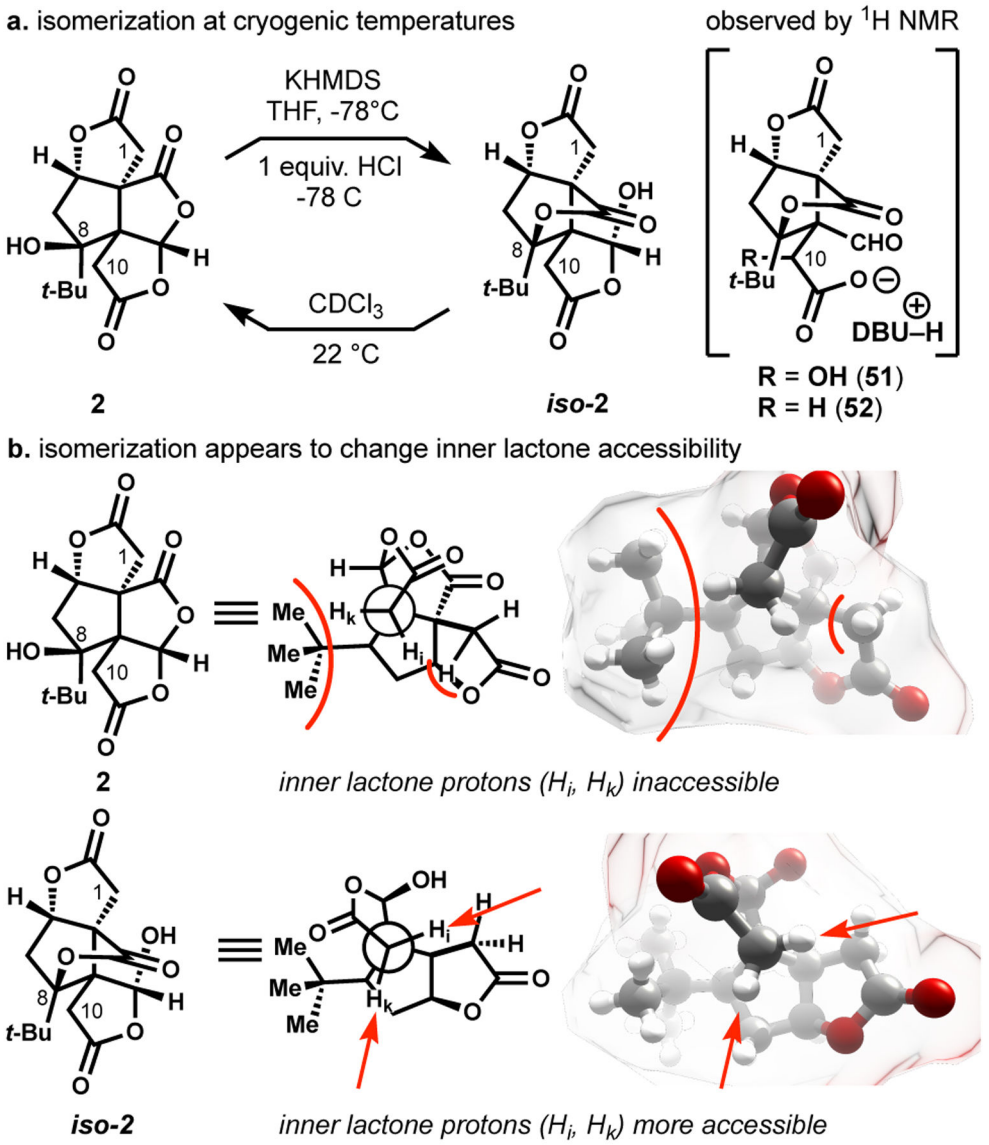

Figure 20.

Does rearrangement to the *iso*-bilobalide skeleton allow access to the inner lactone protons H_i and H_k? **a.** isomerization can be effected with strong base at low temperature or weak base at room temperature (quantitative in 10 min.); **b.** isomerization changes proton accessibility on 180° trajectories of approach.

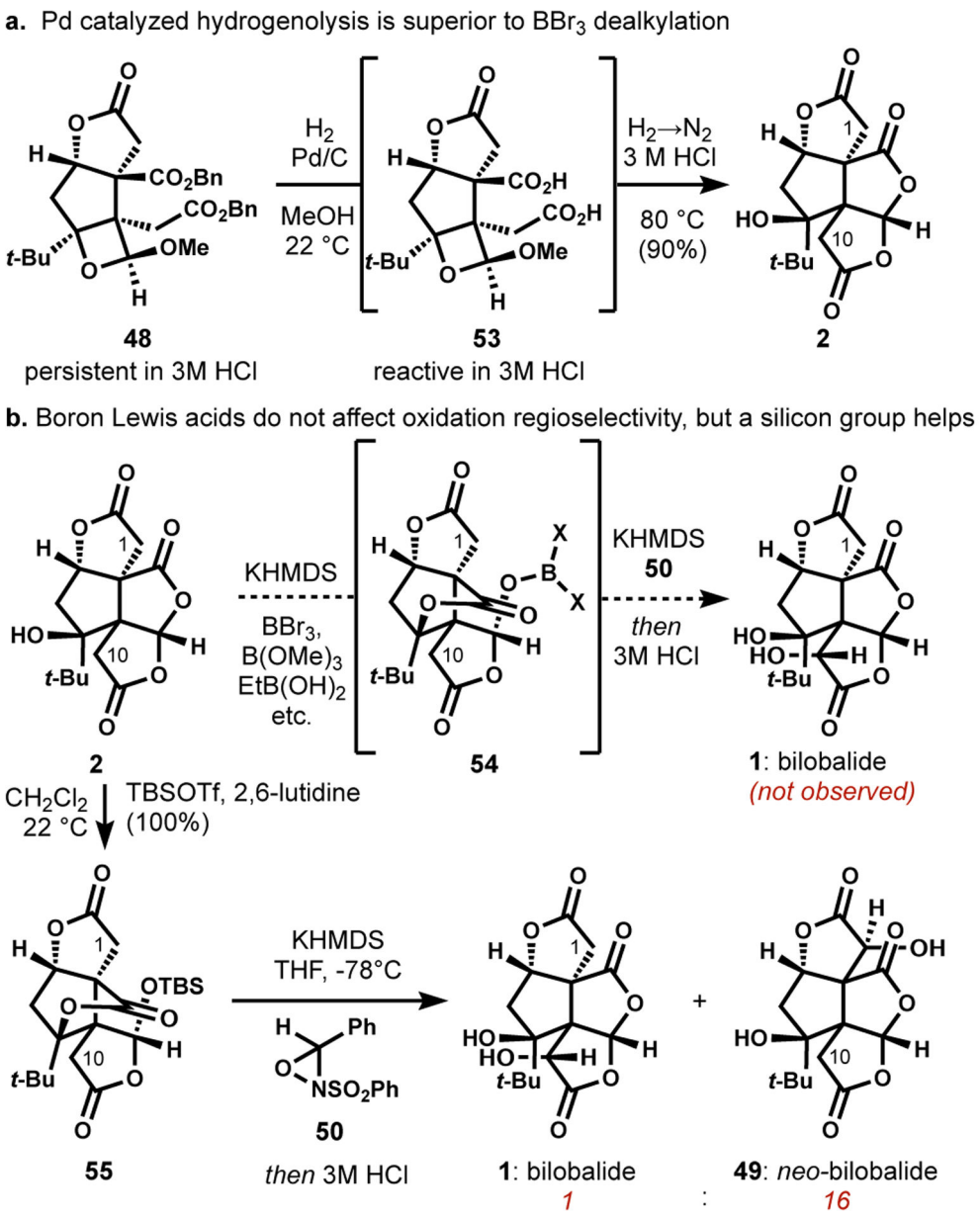

Figure 21.

a. Replacement of BBr_3 in a global deprotection increases yield but removes the boron impurities that may have facilitated C10 hydroxylation; **b.** boron Lewis acids are ineffectual, but an isomerized silyl ether provides a trace of **1**.

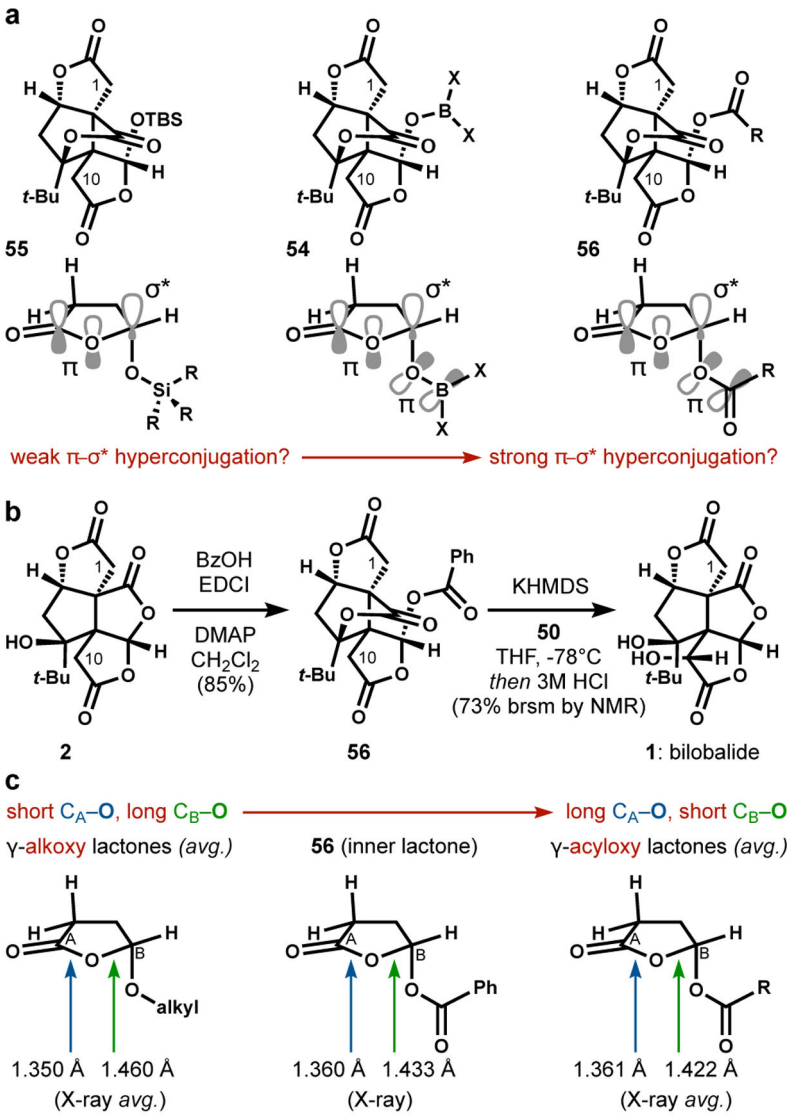

Figure 22a–c.

Did hyperconjugation from an intermediate borate ester acidify the inner lactone? A stable benzoate ester causes selective oxidation of C10 to generate bilobalide (**1**).

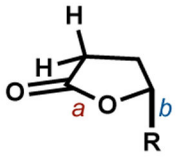

R	*a*	*b*	ΔG_{depr}	pKa	ΔpKa
H	1.35	1.44	27.5	22	0
OTBS	1.36	1.44	27.2	21.8	0.2
$OB(OH)_2$	1.36	1.43	23.2	18.6	3.4
OCOMe	1.36	1.41	21.6	17.3	4.7
OCOPh	1.37	1.41	22.2	17.8	4.2

Figure 22d.

Calculated bond lengths (ångströms) and free energies of deprotonation (kcal/mol) by acetate anion at the ωB97X-D/6-311++G(d,p),SMD(THF)//ωB97X-D/6-31+G(d,p) level of theory.

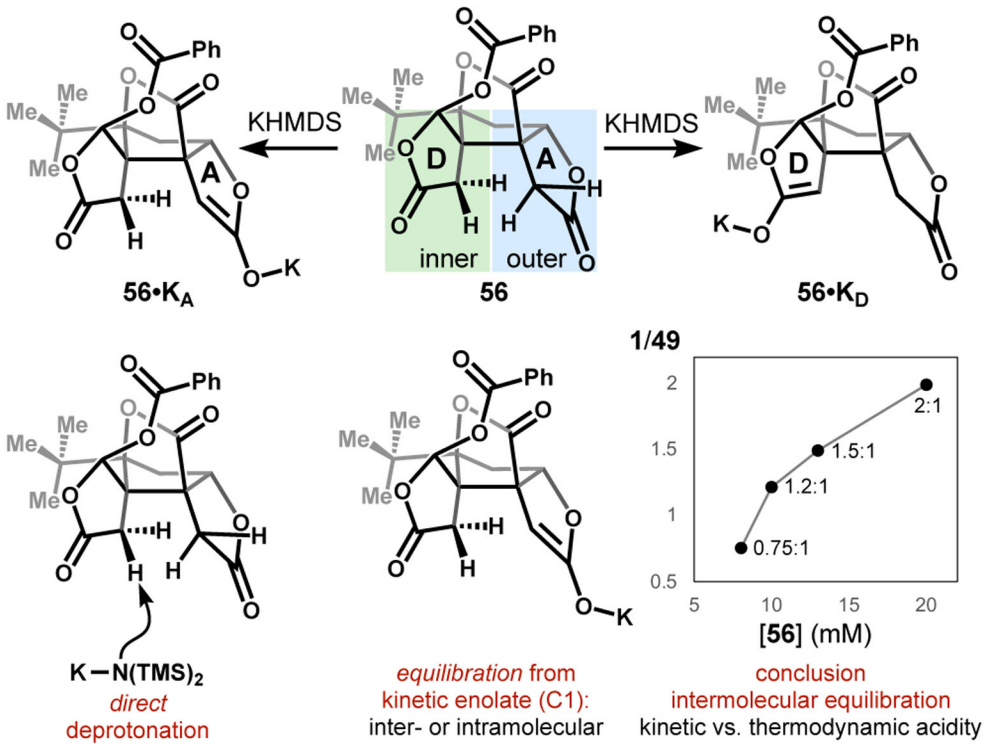

Figure 23.

Addition of **56** (varying concentrations) to a solution of KHMDS and **50** (constant concentration) indicates intermolecular proton transfer and equilibration to a thermodynamic, inner enolate from the kinetic, outer enolate.

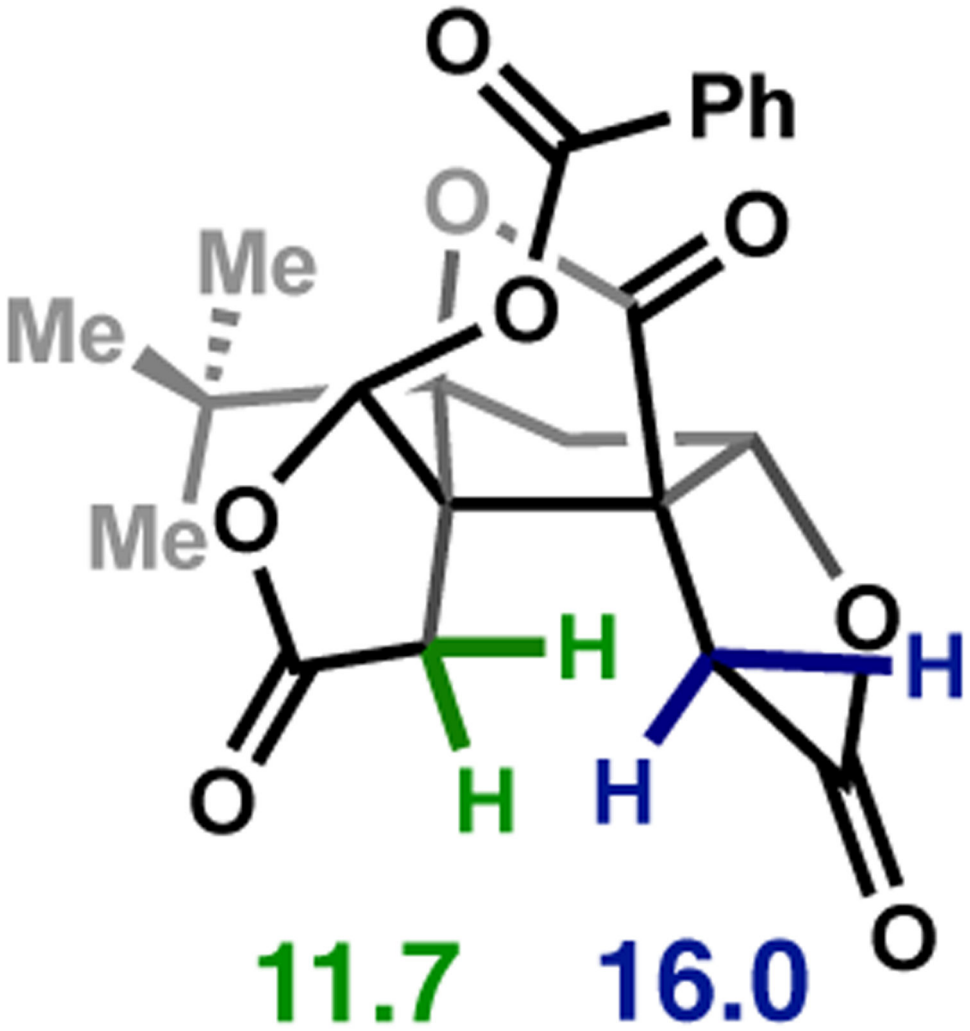

Figure 24.
Calculated free energies (kcal/mol) of deprotonation by acetate anion at the ωB97X-D/6-311++G(d,p), SMD(THF)//ωB97X-D/6-31+G(d,p) level of theory.

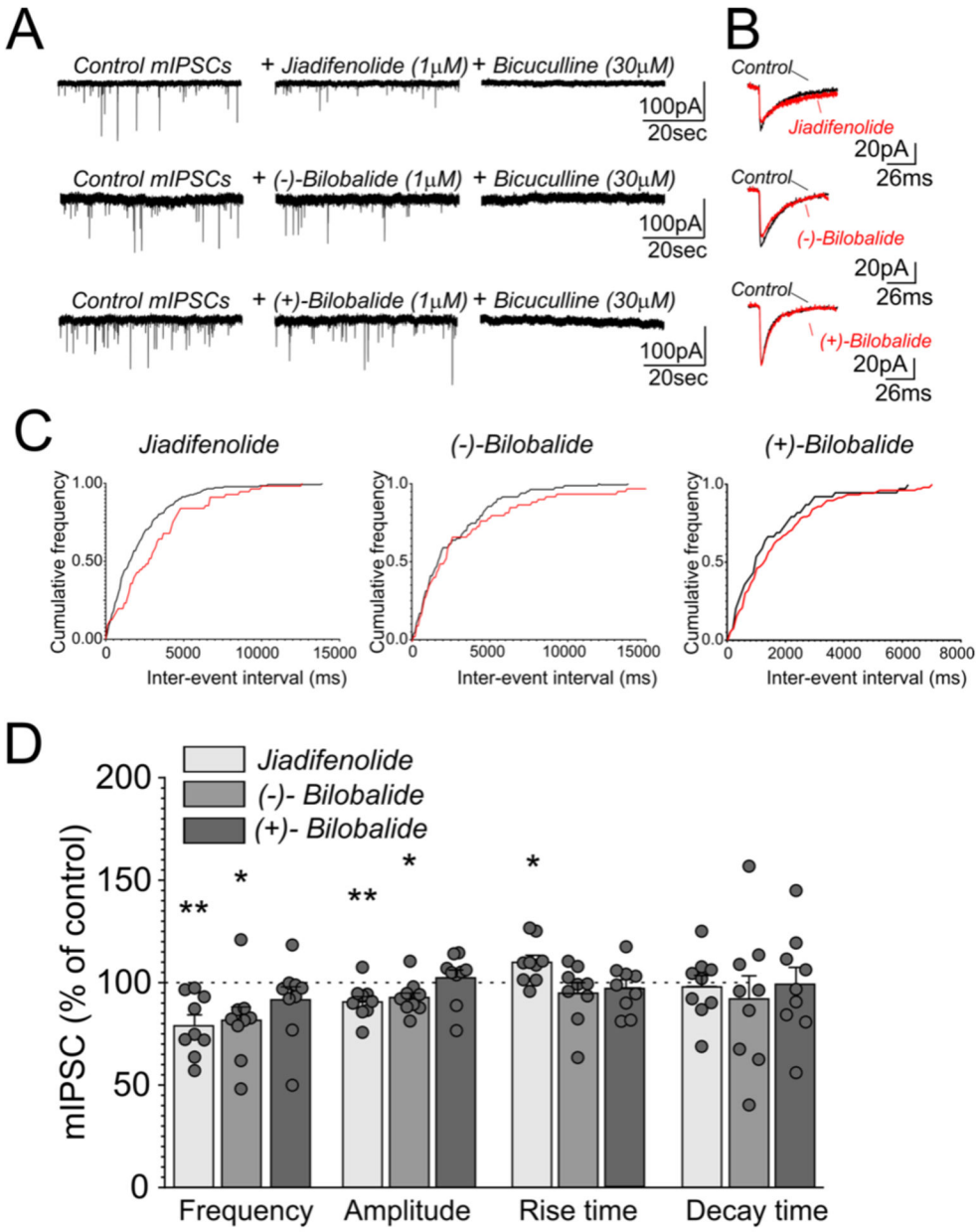

Figure 25.

Effects on spontaneous GABAA receptor mediated neurotransmission in acute brain slices. **a.** representative miniature inhibitory postsynaptic current (mIPSC) recordings in central nucleus of the amygdala (CeA) neurons from naive rats during control (left panel), during superfusion of either jiadifenolide, (−)-bilobalide, or (+)-bilobalide (middle panel; all at 1 μM), and in continued presence of either jiadifenolide, (−)-bilobalide, or (+)-bilobalide, in presence of bicuculline (30μM) confirming the GABAergic nature of the mIPSC are depicted; **b.** scaled mIPSC averages from the traces depicted in panel A before (black trace) and in presence of the indicated compound (red trace) are shown; **c.** cumulative frequency distributions for CeA neurons before (black) and in the presence of the indicated drug are shown; **d.** bars represent means ± S.E.M. from 8-9 individual CeA neurons summarizing the

effects of jiadifenolide, (−)-bilobalide, and (+)-bilobalide on mIPSC frequencies, amplitudes, rise and decay times. Differences to baseline control conditions (indicated as dashed line) were calculated using one-sample t-tests (*/** = $P < 0.05/0.01$).

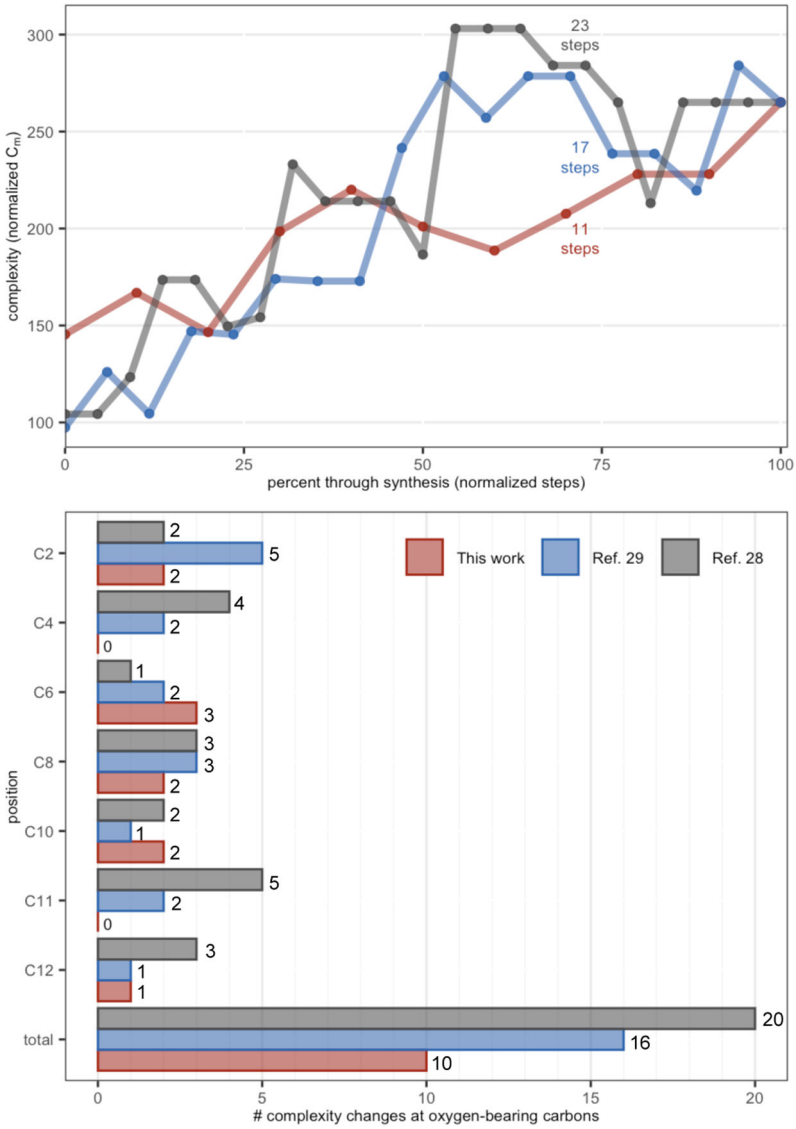

Figure 26.

Different uses of Böttcher scores to annotate changes in complexity over the course of synthesis. **a**. Overshooting complexity is correlated to longer syntheses; **b.** number of complexity changes at each oxidized carbon is directly related to number of total steps.

Table 1.

Reversible and irreversible enolization conditions favor starting materials over product.

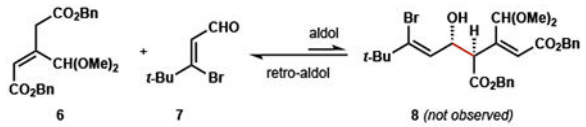

entry	conditions	result
1	LDA, THF −78 °C	**6** recovered
2	Li, Na, or KHMDS, THF −78 °C	**6** recovered
3	Cs_2CO_3	**6** recovered
4	$MgCl_2$, NEt_3, TBSCl	trace **8**
5	**treatment of 8 with Et_3N**	**6**